




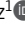


## ARTICLE

# The transcription factor NFAT5 limits infection-induced type I interferon responses

Hector Huerga Encabo<sup>1</sup> , Laia Traveset<sup>1</sup>, Jordi Argilaguet<sup>2</sup> , Ana Angulo<sup>3</sup>, Estanislao Nistal-Villán<sup>4</sup> , Rahul Jaiswal<sup>5</sup>, Carlos R. Escalante<sup>5</sup>, Christos Gekas<sup>6</sup>, Andreas Meyerhans<sup>2,7</sup> , Jose Aramburu<sup>1</sup> , and Cristina López-Rodríguez<sup>1</sup> 

**Type I interferon (IFN-I) provides effective antiviral immunity but can exacerbate harmful inflammatory reactions and cause hematopoietic stem cell (HSC) exhaustion; therefore, IFN-I expression must be tightly controlled. While signaling mechanisms that limit IFN-I induction and function have been extensively studied, less is known about transcriptional repressors acting directly on IFN-I regulatory regions. We show that NFAT5, an activator of macrophage pro-inflammatory responses, represses Toll-like receptor 3 and virus-induced expression of IFN-I in macrophages and dendritic cells. Mice lacking NFAT5 exhibit increased IFN-I production and better control of viral burden upon LCMV infection but show exacerbated HSC activation under systemic poly(I:C)-induced inflammation. We identify IFN $\beta$  as a primary target repressed by NFAT5, which opposes the master IFN-I inducer IRF3 by binding to an evolutionarily conserved sequence in the *IFNB1* enhancosome that overlaps a key IRF site. These findings illustrate how IFN-I responses are balanced by simultaneously opposing transcription factors.**

## Introduction

The involvement of type I IFN (IFN-I) in promoting diverse immunopathologies highlights the need for understanding mechanisms that repress its expression. However, while signal transduction mechanisms that limit IFN-I production or function are quite well characterized, less is known about transcription repressors that control IFN-I genes by acting directly on their genomic regulatory regions (Arimoto et al., 2018; Levy et al., 2011), and few direct repressors, such as activating transcription factor 3 (ATF3; Labzin et al., 2015) and IFN regulatory factor 2 (IRF2; Senger et al., 2000), have been studied in detail. IFN-I plays a central role in the protection against pathogens such as viruses (McNab et al., 2015; Ivashkiv and Donlin, 2014) but is also a potent driver of autoinflammatory and autoimmune diseases. Exacerbated inflammatory responses can damage tissues, enhance activation of pattern-recognition receptors (PRRs), and lead to increased and persistent IFN-I production (Rodero and Crow, 2016; Theofilopoulos et al., 2005). The physiopathological role of IFN-I extends to other scenarios such as the exhaustion of adaptive immune responses during chronic viral infections, the control of tumor progression, and the activation of hematopoietic stem cells (HSCs) in response to inflammatory stress (King and Goodell, 2011; Zitvogel et al., 2015; Snell and Brooks, 2015).

IFN-I comprises IFN $\beta$ , different forms of IFN $\alpha$ , and other IFN types (Pestka et al., 2004), all of which can be expressed in response to PRRs such as particular transmembrane TLRs and cytosolic RNA and DNA sensors (Akira et al., 2006; Wu and Chen, 2014) that detect molecular patterns from pathogens and damaged cells. IFN-I signals through the IFN $\alpha/\beta$  receptor (IFNAR) to induce the expression of numerous IFN-stimulated genes (ISGs), encoding proteins that modulate the viral life cycle or work as positive and negative regulators of the response to IFN-I (MacMicking, 2012; Schneider et al., 2014). Expression of IFN-I is orchestrated by diverse transcription regulators, among which IRF3, IRF7, and p65/NF- $\kappa$ B are the key factors that recognize the regulatory regions of IFN-I genes and induce their expression upon PRR activation in cells such as conventional and plasmacytoid dendritic cells (pDCs), macrophages, and fibroblasts (McNab et al., 2015; Ivashkiv and Donlin, 2014; Honda et al., 2006). Transcription of *Ifnb1* is the best-characterized paradigm for IFN-I induction, with a short promoter region containing a central 50-bp element known as the IFN $\beta$  enhancosome, which is recognized by IRF3, IRF7, and p65/NF- $\kappa$ B (Panne et al., 2007). In parallel to the characterization of transcriptional activators of IFN-I, studies have identified numerous

<sup>1</sup>Immunology Unit, Department of Experimental and Health Sciences, Universitat Pompeu Fabra, Barcelona, Spain; <sup>2</sup>Infection Biology Laboratory, Department of Experimental and Health Sciences, Universitat Pompeu Fabra, Barcelona, Spain; <sup>3</sup>Immunology Unit, Department of Biomedical Sciences, Medical School, University of Barcelona, Barcelona, Spain; <sup>4</sup>Microbiology Section, Departamento de Ciencias, Farmacéuticas y de la Salud, Facultad de Farmacia, Universidad CEU San Pablo, CEU Universities, Madrid, Spain; <sup>5</sup>Department of Physiology and Biophysics, Virginia Commonwealth University School of Medicine, Richmond, VA; <sup>6</sup>Program in Cancer Research, Institut Hospital del Mar d'Investigacions Mèdiques, Barcelona, Spain; <sup>7</sup>Institució Catalana de Recerca i Estudis Avançats, Barcelona, Spain.

Correspondence to Cristina López-Rodríguez: [cristina.lopez-rodriguez@upf.edu](mailto:cristina.lopez-rodriguez@upf.edu).

© 2019 Huerga Encabo et al. This article is distributed under the terms of an Attribution–Noncommercial–Share Alike–No Mirror Sites license for the first six months after the publication date (see <http://www.rupress.org/terms/>). After six months it is available under a Creative Commons License (Attribution–Noncommercial–Share Alike 4.0 International license, as described at <https://creativecommons.org/licenses/by-nc-sa/4.0/>).

negative regulators that act on PRR-regulated signaling components and also downstream IFNAR (Arimoto et al., 2018), underscoring the importance of a tight control of IFN-I responses to prevent their potentially pathogenic effects. In this context, though, our knowledge about transcription regulators that could directly repress IFN-I expression is still quite limited (Arimoto et al., 2018; Levy et al., 2011; Ivashkiv and Donlin, 2014).

NFAT5 is a transcription factor of the Rel family with homology to NF- $\kappa$ B and calcineurin-activated NFATc proteins. NFAT5 modulates diverse immune functions in myeloid cells and lymphocytes in basal conditions and in response to pathogen receptors, cytokines, and hypertonic stress (Aramburu and López-Rodríguez, 2019). NFAT5 is constitutively expressed in macrophages and is further induced and activated by TLR through the IKK $\beta$ -NF- $\kappa$ B pathway to promote expression of diverse pro-inflammatory genes (Buxadé et al., 2012; Aramburu and López-Rodríguez, 2019). This function of NFAT5, which can be enhanced by hypertonic stress, supports the classical polarization of macrophages and also protects against *Leishmania* infection in vivo (Buxadé et al., 2012; Jantsch et al., 2015; Tellechea et al., 2018). While NFAT5 can be inducibly recruited to promoters of target genes, such as *Nos2* and *Il6* upon TLR activation, it can also be constitutively bound to regulatory regions of other genes in basal conditions as shown for the master MHCII regulatory factor *Ciita* (Buxadé et al., 2012, 2018). PRR activation induces many types of gene products in addition to prototypical inflammatory cytokines, and receptors such as TLR3 also induce IFN-I expression (Akira et al., 2006; Wu and Chen, 2014). In this work, we report that NFAT5 represses IFN-I transcription, and thus attenuates IFN-I-dependent responses, and identify IFN $\beta$  transcription as a primary target for NFAT5. We found that NFAT5 binds the *Ifnb1* enhanceosome in a TLR3-dependent manner to prevent IRF3 binding and inhibit IFN $\beta$  promoter activity. Expression of IFN-I and ISG was amplified in NFAT5-deficient macrophages, DCs, and fibroblasts upon viral infection or direct TLR3 stimulation with poly(I:C) (polyinosinic-polycytidylic acid). NFAT5-deficient mouse models reacted to poly(I:C)-induced systemic inflammation with increased IFN-I-mediated activation of their HSCs, and responded to viral infection with enhanced stimulation of the IFN-I pathway and improved control of viral load.

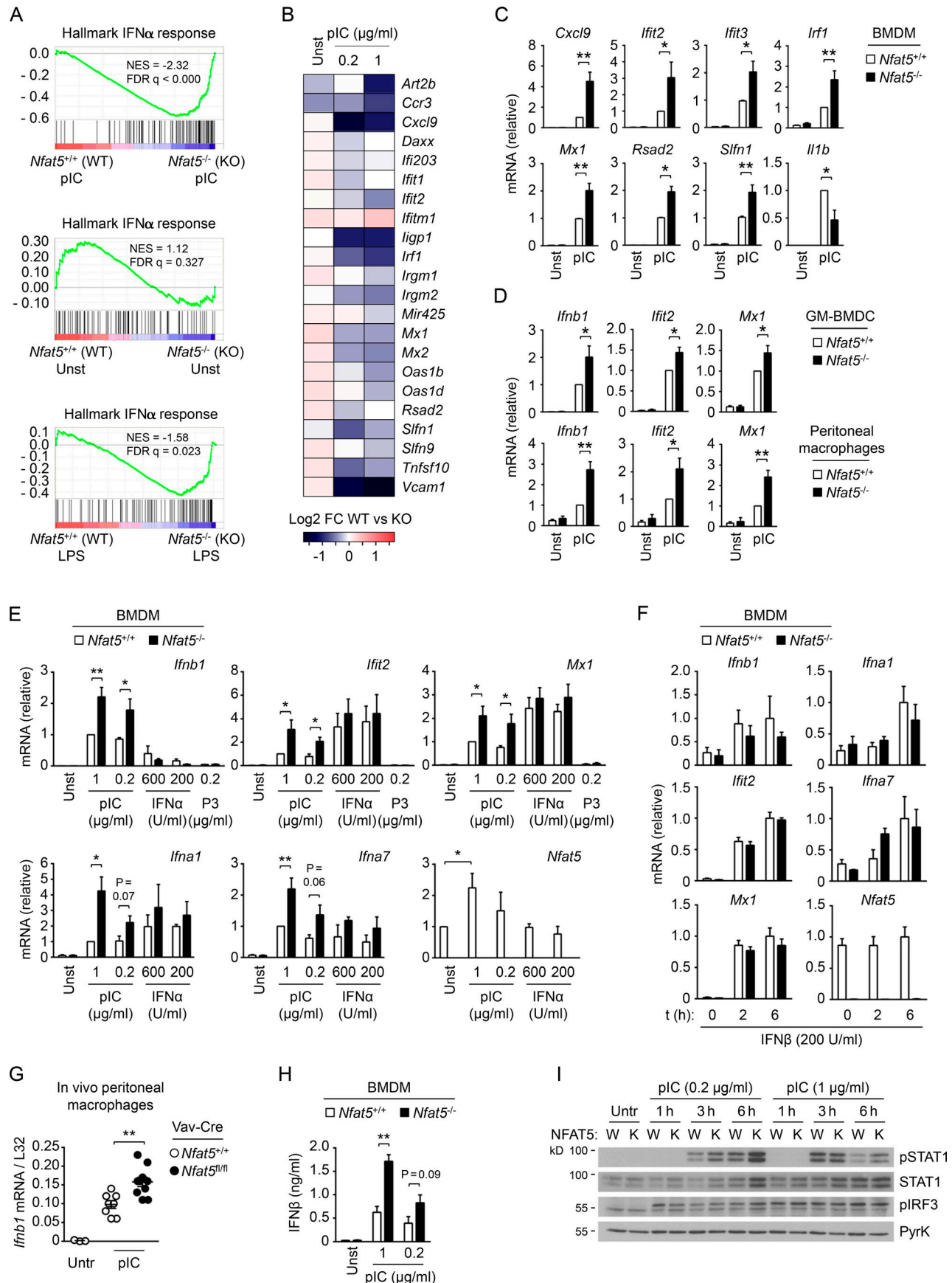
## Results

### NFAT5 inhibits TLR3-induced IFN-I responses in macrophages and DCs

Previous work has shown that NFAT5 induces diverse pro-inflammatory genes in response to TLRs and classical macrophage polarization (Buxadé et al., 2012; Tellechea et al., 2018). Gene set enrichment analysis (GSEA) of a previously published NFAT5-regulated transcriptome in macrophages stimulated with the TLR4 ligand LPS (Buxadé et al., 2012) identified enhanced expression of ISGs in NFAT5-deficient macrophages (Fig. 1 A, bottom). Intrigued by this finding, we explored the potential contribution of NFAT5 to IFN-I responses in macrophages stimulated with poly(I:C), a synthetic double-strand RNA

that activates endosomal TLR3 when added directly to the culture medium. TLR3 engages the TRIF adaptor-dependent signaling pathway and induces robust IFN-I expression by activating p65/NF- $\kappa$ B, IRF3, and IRF7 (O'Neill and Bowie, 2007; Oshiumi et al., 2003; Yamamoto et al., 2003). GSEA of microarray experiments with poly(I:C)-treated, NFAT5-deficient bone marrow-derived macrophages (BMDMs) revealed a global upregulation of IFN-I response genes with respect to wild-type BMDMs (Fig. 1 A, top), but not other TLR3-regulated responses such as the apoptosis gene set (Fig. S1 A). Macrophages did not display any NFAT5-sensitive IFN-I response in the absence of poly(I:C) stimulation (Fig. 1 A, middle). The GSEA also identified an enhanced IFN $\gamma$  (type II IFN) signature in poly(I:C)-treated, NFAT5-deficient BMDMs, consistent with the similar gene expression patterns shared by type I and II IFN responses (Fig. S1 A). Almost half of the genes differentially expressed between poly(I:C)-treated NFAT5-deficient and wild-type macrophages (1,209 out of 2,731) were annotated in the Interferome database as responsive to IFN-I (Interferome database v2.01; Rusinova et al., 2013), and from these, 62% were upregulated in NFAT5-deficient cells (Fig. 1 B, Fig. S1 B, and Table S1). Lack of NFAT5 did not affect the expression of diverse genes encoding for components of the TLR3 signaling pathway (*Tlr3* itself, *Ticam1*/*Trifl*, *Traf3*, *Traf6*, *Ripk1*, *Tbk1*, *Ikbke*, *Irf3*, and *Irf7*, among others) or the IFN-I receptor (*Ifnar1*, *Ifnar2*, *Jak1*, and *Jak2*, among others) in macrophages stimulated with poly(I:C) (Table S2). Altogether, the analysis of these RNA datasets revealed an unexpected duality in the function of NFAT5, since in addition to facilitating expression of prototypical pro-inflammatory genes upon TLR stimulation (Buxadé et al., 2012), it could also restrain IFN-I responses.

We next used real-time quantitative PCR (RT-qPCR) to compare the expression of *Ifnb1* and various ISGs in BMDMs, bone marrow-derived DCs (BMDCs), and freshly isolated peritoneal macrophages and observed that lack of NFAT5 caused a significant increase in the induction of these genes in the three populations upon poly(I:C) treatment (Fig. 1, C and D), indicating a widespread role for NFAT5 in limiting IFN-I responses. We also analyzed NFAT5-deficient macrophages for their response to IFN $\alpha$  (IFN $\alpha$ 4) and Pam3CSK, a TLR2 agonist that induces NFAT5 expression and activation (Buxadé et al., 2012), but does not induce IFN-I responses in macrophages. Compared with the NFAT5-inhibited *Ifnb1*, *Ifna1*, *Ifna7*, and ISG (*Ifit2* and *Mx1*) expression upon poly(I:C) stimulation, induction of these genes by IFN $\alpha$  was not repressed by NFAT5, and Pam3CSK did not induce them (Fig. 1 E). Similarly, IFN $\beta$ -induced robust expression of ISGs and modest induction of IFN-I genes in macrophages were independent of NFAT5 (Fig. 1 F). In line with these findings, poly(I:C) treatment in vivo caused exacerbated *Ifnb1* expression in peritoneal macrophages (CD11b<sup>+</sup> cells) of mice lacking NFAT5 in immune cells (*Nfat5*<sup>fl/fl</sup> Vav-Cre; Fig. 1 G). NFAT5-deficient BMDMs also produced significantly more IFN $\beta$  protein in response to poly(I:C) (Fig. 1 H), and this was associated with increased phosphorylation and upregulation of STAT1 upon IFNAR activation (Fig. 1 I and Fig. S1 E). However, we did not detect obvious differences between wild-type and NFAT5-deficient BMDMs in TLR3-induced phosphorylation of IRF3, the master



**Figure 1. NFAT5 inhibits TLR3-induced IFN-I responses in macrophages and DCs.** (A) GSEA of Hallmark database for the IFN $\alpha$  response from microarray data comparing wild-type (*Nfat5*<sup>+/+</sup>, WT) and NFAT5-deficient (*Nfat5*<sup>-/-</sup>, knockout [KO]) BMDMs unstimulated (middle), stimulated with poly(I:C) (pIC; 1  $\mu$ g/ml, 6 h; top), or stimulated with LPS (0.3 ng/ml, 6 h; bottom). NES, normalized enrichment score; FDR, false discovery rate. (B) Heat map illustrating the differential expression of a set of ISGs in *Nfat5*<sup>+/+</sup> WT and *Nfat5*<sup>-/-</sup> KO BMDMs in basal conditions (Unst) or in response to poly(I:C) stimulation (pIC; 0.2 and 1  $\mu$ g/ml, 6 h; see Table S1 for an extended list of genes responsive to IFN $\alpha$  and  $\beta$  differentially expressed between poly(I:C)-stimulated wild-type and NFAT5-deficient BMDMs). Log2 FC, fold-change in log2. (C) RT-qPCR analysis of the indicated ISGs and the NFAT5-induced *Iilb* in *Nfat5*<sup>+/+</sup> and *Nfat5*<sup>-/-</sup> BMDMs in basal conditions and after 6 h of stimulation with 1  $\mu$ g/ml of poly(I:C). (D) RT-qPCR analysis of *Ifnb1* and the ISGs *Ifit2* and *Mx1* in *Nfat5*<sup>+/+</sup> and *Nfat5*<sup>-/-</sup> BMDCs differentiated with GM-CSF (GM-BMDCs), and peritoneal macrophages left unstimulated or stimulated with poly(I:C) (1  $\mu$ g/ml, 6 h). (E) RT-qPCR analysis of IFN-I genes, ISGs *Ifit2* and *Mx1*, and *Nfat5* in *Nfat5*<sup>+/+</sup> and *Nfat5*<sup>-/-</sup> BMDMs in basal conditions and after 6 h of stimulation with poly(I:C), IFN $\alpha$  or Pam3CSK (P3). (F) mRNA expression of the indicated genes in *Nfat5*<sup>+/+</sup> and *Nfat5*<sup>-/-</sup> BMDMs in basal conditions and after stimulation with IFN $\beta$  for 2 and 6 h. (G) RT-qPCR analysis of *Ifnb1* mRNA expression in peritoneal macrophages isolated from mice with a conditional deletion of *Nfat5* in immune cells (*Nfat5*<sup>fl/fl</sup> Vav-Cre) or control littermates (*Nfat5*<sup>+/+</sup> Vav-Cre) after in vivo poly(I:C) injection (10 mg/kg, 6 h). (H) IFN $\beta$  production measured by ELISA in the supernatants of *Nfat5*<sup>+/+</sup> and *Nfat5*<sup>-/-</sup> BMDMs in basal conditions and after 24 h of poly(I:C) stimulation. (I) Western blot analysis for the indicated proteins in *Nfat5*<sup>+/+</sup> (W) and *Nfat5*<sup>-/-</sup> (K) BMDMs left unstimulated or stimulated with poly(I:C) as indicated. All mRNA values were normalized to *L32*. Error bars in C–H show the mean  $\pm$  SEM. Data in A and B are from three independent experiments, each comparing cells from one NFAT5-deficient mouse and one wild-type littermate. Results in C–F are from seven (C), five (D), four to five (E), and three (F) independent experiments, each comparing cells from one NFAT5-deficient mouse and one wild-type littermate. Results in G are from three independent experiments and comprise three untreated wild-type, eight poly(I:C)-treated wild-type, and 10 NFAT5-deficient mice. Results in H are from two independent experiments, each comparing cells from two NFAT5-deficient mice and two wild-type littermates. The Western blot in I is representative of two independent experiments (see Fig. S1 E). Statistical significance in C and D was determined with: a one-sample *t* test using wild-type cells stimulated with 1  $\mu$ g/ml poly(I:C) as reference with a value of 1; in E with a one-sample *t* test for comparisons with the reference sample and an unpaired *t* test for comparisons between other samples; and in G and H with an unpaired *t* test. \*, *P* < 0.05; \*\*, *P* < 0.01.

regulator of IFN-I transcription (Fig. 1 I). NFAT5 itself accumulated in macrophages upon prolonged poly(I:C) treatment but not by direct IFN-I (IFN $\alpha$  or IFN $\beta$ ) stimulation (Fig. 1, E and F; and Fig. S1 C; Buxadé et al., 2012), and indeed, TLR3-induced NFAT5 accumulation was IFNAR-independent (Fig. S1 D). Altogether, this set of results showed that NFAT5 repressed IFN-I expression in macrophages and DCs activated by TLR3, but not upon direct stimulation with IFN-I, which suggested that NFAT5 acted upon TLR3 activation but not upon direct IFNAR activation.

#### Enhanced IFN-I production and viral clearance upon lymphocytic choriomeningitis virus (LCMV) infection in mice lacking NFAT5

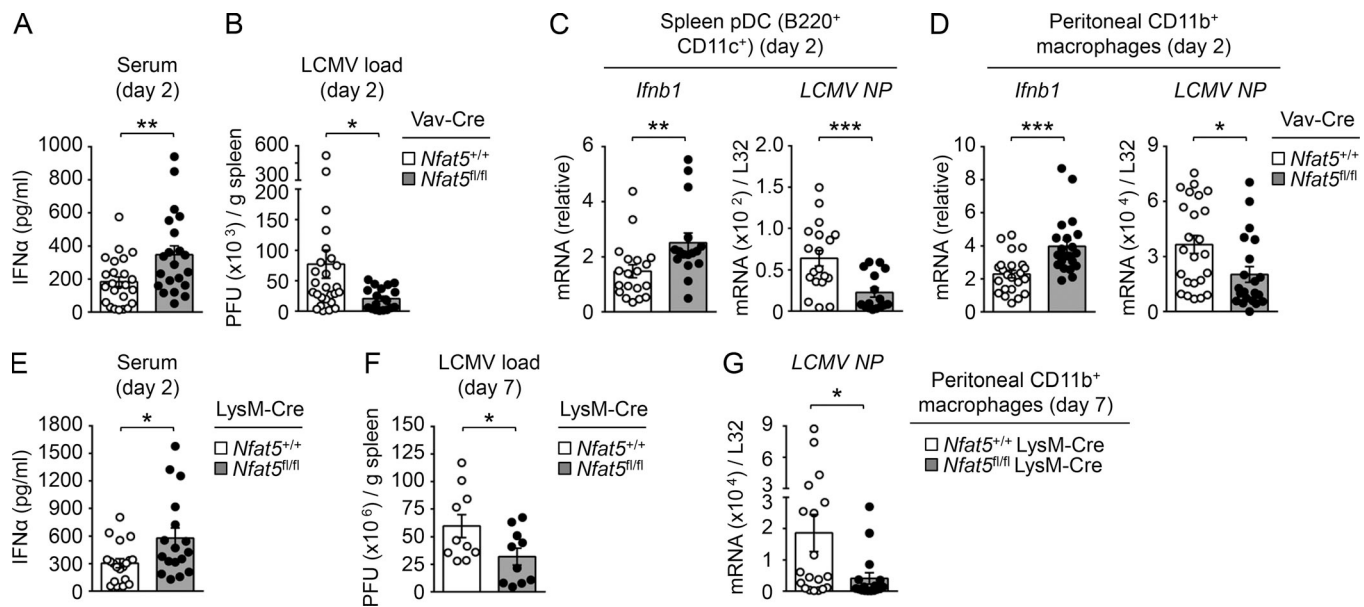
In view of these results, we asked about the biological impact of NFAT5 on IFN-I responses during a viral infection in vivo. We assessed this in a mouse model of infection with LCMV, a single-stranded RNA virus that activates different TLR and cytosolic RNA sensors (Borrow et al., 2010). C57BL/6 mice infected with a low dose of LCMV strain Docile developed a self-resolving acute infection that starts to be controlled around day 9 (Moskophidis et al., 1993). This infection model causes a rapid and transient burst of IFN-I that is required to control viral replication, prime virus-specific CD8<sup>+</sup> T lymphocytes, and prevent their exhaustion (Merigan et al., 1977; Cousens et al., 1999; Borrow et al., 2010; Ng et al., 2013). We therefore sought to analyze the early phase of the response to acute viral infection in mice lacking NFAT5 in immune cells (*Nfat5*<sup>fl/fl</sup> Vav-Cre) using a low dose (2  $\times$  10<sup>2</sup> PFU per mouse) of the LCMV strain Docile. Compared with control littermates, *Nfat5*<sup>fl/fl</sup> Vav-Cre mice showed enhanced levels of IFN $\alpha$  in serum 2 d after infection (Fig. 2 A) and improved control of their viral load (Fig. 2 B). Analysis of spleen pDCs (CD11c<sup>+</sup> B220<sup>+</sup>; Fig. 2 C and Fig. S2 A), peritoneal macrophages (CD11b<sup>+</sup>; Fig. 2 D), and bone marrow pDCs (CD11c<sup>+</sup> B220<sup>+</sup>) and macrophages (CD11b<sup>+</sup> F4/80<sup>+</sup>; Fig. S2, B–D) isolated 2–3 d after infection showed increased expression of

*Ifnb1* and different ISGs in *Nfat5*<sup>fl/fl</sup> Vav-Cre mice, together with reduced expression of the LCMV nucleoprotein gene (*LCMV NP*). In parallel, we confirmed that percentages of pDCs and macrophages were similar in spleens and bone marrow of infected *Nfat5*<sup>fl/fl</sup> Vav-Cre and control mice (Fig. S2 E). We next used myeloid-specific NFAT5-deficient mice (*Nfat5*<sup>fl/fl</sup> LysM-Cre) to avoid a potential contribution of NFAT5 in T lymphocytes (Alberdi et al., 2017) when analyzing a later time point after acute LCMV infection. These mice also presented increased IFN $\alpha$  production 2 d after infection (Fig. 2 E) and maintained better clearance of their viral load in spleen and peritoneal macrophages 5 d later (Fig. 2, F and G), at the peak of viral burden and when IFN-I is nearly undetectable (Moskophidis et al., 1993; Merigan et al., 1977; Borrow et al., 2010). Therefore, these acute infection experiments showed that lack of NFAT5 in macrophages and pDCs enhanced IFN-I production and improved viral clearance in vivo.

#### NFAT5 represses IFN-I responses in macrophages and DCs infected with different viruses

We next asked whether NFAT5 could control the IFN-I pathway upon direct infection of DCs and macrophages by viruses that have different functional characteristics and activate different PRRs. First, we observed that macrophages infected with vesicular stomatitis virus (VSV) or murine CMV (MCMV) accumulated *Nfat5* mRNA, which reached a maximal expression at 24 h (Fig. 3 A, left panels). Analysis of the response of NFAT5-deficient macrophages (BMDMs) and GM-CSF-induced conventional bone marrow-derived myeloid DCs (GM-BMDCs) to VSV or MCMV showed that they expressed higher levels of *Ifnb1*, *Ifit2*, and *Mx1* compared with control cells coinciding with the peak of the response 12 h after infection (Fig. 3, A and B). Similarly, NFAT5-deficient Flt3 ligand (Flt3L)-induced conventional (CD11c<sup>+</sup> CD11b<sup>+</sup>) and plasmacytoid (CD11c<sup>+</sup> B220<sup>+</sup>) BMDCs responded to VSV or LCMV infection with increased expression of different IFN-I genes (*Ifnb1*, *Ifna1*, and *Ifna7*) and *Ifit2* (Fig. 3 C and





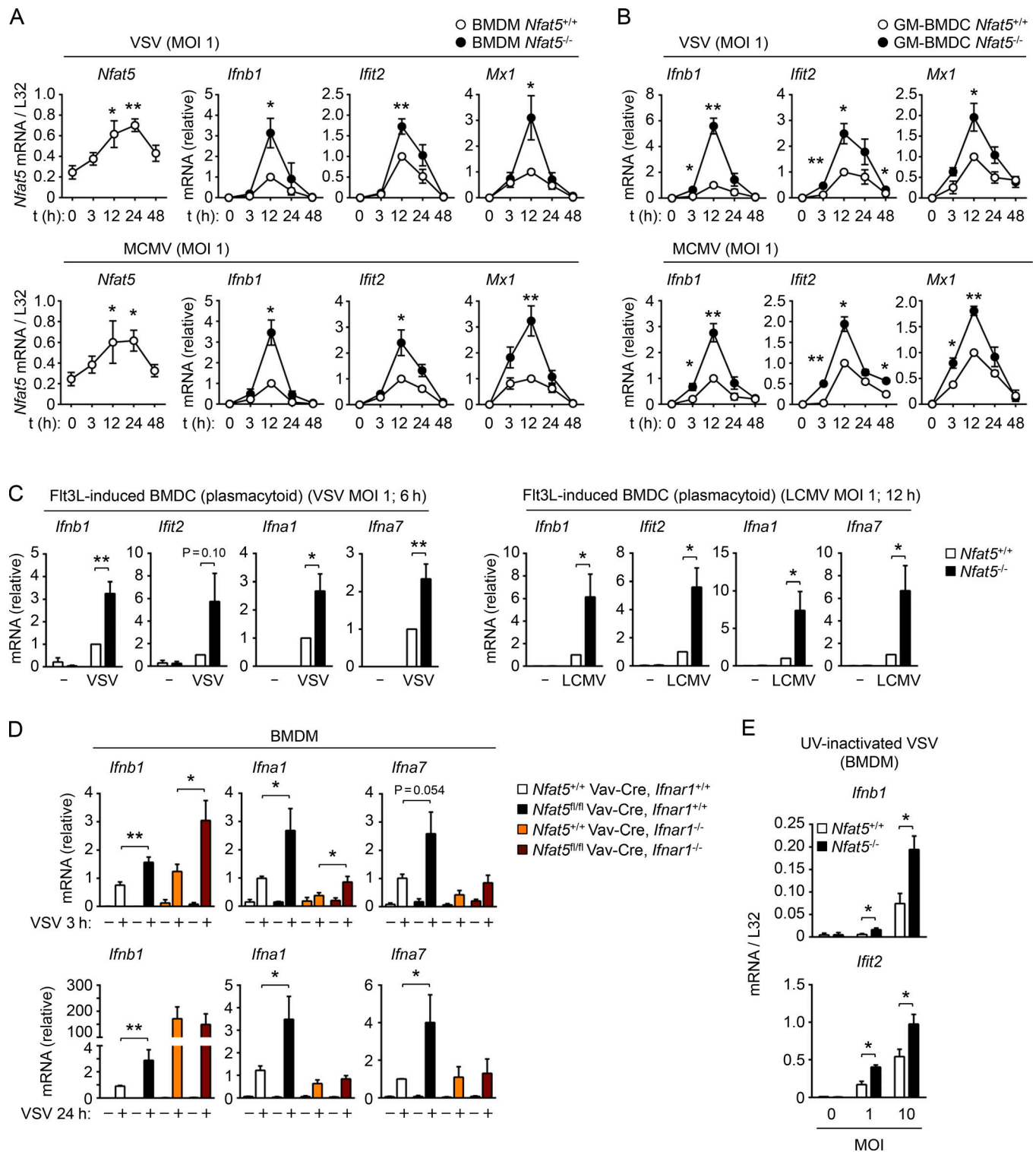
**Figure 2. Enhanced IFN-I production and viral clearance upon LCMV infection in NFAT5-deficient mouse models. (A and B)** Analysis of IFNα concentration in serum (A) and viral load in the spleens (B) of *Nfat5*<sup>+/+</sup> Vav-Cre (*n* = 24) and *Nfat5*<sup>fl/fl</sup> Vav-Cre (*n* = 21) mice 2 d after acute infection with LCMV strain Docile ( $2 \times 10^2$  PFU per mouse). **(C and D)** mRNA levels of *Ifnb1* and the viral gene *LCMV NP* in splenic pDCs (C) and peritoneal macrophages (D) of *Nfat5*<sup>+/+</sup> Vav-Cre (*n* = 19) and *Nfat5*<sup>fl/fl</sup> Vav-Cre (*n* = 16) mice 2 d after infection. pDCs were isolated by flow cytometry cell sorting using the gating strategy shown in Fig. S2 A. **(E–G)** Analysis of IFNα concentration in serum (day 2; E), viral load in spleen (day 7; F), and mRNA levels of the viral gene *LCMV NP* in peritoneal macrophages (day 7; G) in *Nfat5*<sup>+/+</sup> LysM-Cre (*n* = 19 in E and G; *n* = 10 in F) and *Nfat5*<sup>fl/fl</sup> LysM-Cre (*n* = 17 in E and G; *n* = 10 in F) mice after acute infection with LCMV. Error bars in A–G show the mean ± SEM. Data in A–D comprise three independent in vivo infection experiments. Data in E–G comprise two independent in vivo infection experiments. Statistical significance was determined with an unpaired *t* test. \*, *P* < 0.05; \*\*, *P* < 0.01; \*\*\*, *P* < 0.001.

Fig. S2 F). Our previous experiments showed that lack of NFAT5 did not affect IFN-I expression in macrophages stimulated with IFNα or IFNβ (Fig. 1, E and F), which suggested that NFAT5 would not repress IFN-I expression downstream IFNAR. We thus assessed whether inhibition of IFN-I expression by NFAT5 in the course of viral infection involved IFNAR signaling. For this, we compared the induction of *Ifnb1* and the α IFNs *Ifna1* and *Ifna7* upon VSV infection of wild-type, NFAT5-deficient, IFNAR-deficient, and double NFAT5- and IFNAR-deficient macrophages. We found that IFN-I repression by NFAT5 was mainly independent of IFNAR early after infection (3 h), whereas at later time points (24 h), maintenance of enhanced IFN-I induction in NFAT5-deficient cells was IFNAR dependent (Fig. 3 D). These experiments indicated that lack of NFAT5 enhanced an early wave of IFNAR-independent IFN-I production, which then sustained prolonged IFN-I expression through IFNAR. From this result, we expected that enhanced IFN-I production in NFAT5-deficient infected cells would lead to increased expression of ISGs in nearby noninfected cells through paracrine IFN-I action. To test this, we infected BMDM with GFP-expressing VSV and analyzed expression of IFN-I and ISGs in infected (GFP<sup>+</sup>) and noninfected (GFP<sup>-</sup>) cells. We confirmed that NFAT5-deficient BMDM expressed more IFN-I than wild-type cells, which led to elevated expression of ISGs *Mx1* and *Ifit2* in noninfected cells in cultures of macrophages lacking NFAT5 (Fig. S2 G). Finally, to exclude a role for NFAT5 in viral replication that could influence our results, we performed infections using UV-inactivated VSV. These experiments showed that NFAT5-deficient macrophages also presented increased IFN-I responses to UV-inactivated VSV

(Fig. 3 E), supporting a role for NFAT5 in restraining the activation of the IFN-I pathway upon sensing pathogens.

#### Exacerbated IFN-I response in NFAT5-deficient mouse models causes enhanced activation of HSCs

One effect of systemic production of IFN-I is the activation of HSCs. This is one of the many effects that infection causes in the immune system, and it can be readily analyzed upon acute poly(I:C) treatment of mice, which is the model of choice for studying IFN-I-mediated HSC activation (Essers et al., 2009; Pietras et al., 2014; Sato et al., 2009). Poly(I:C) injection induced an early accumulation of IFNα in serum that was more pronounced in mice deficient for NFAT5 in immune cells (*Nfat5*<sup>fl/fl</sup> Vav-Cre; Fig. 4 A) or myeloid cells (*Nfat5*<sup>fl/fl</sup> LysM-Cre; Fig. 4 B). Acute poly(I:C) treatment consisted of two consecutive poly(I:C) injections 48 h apart, and short-term effects were analyzed 24 h later, as in Essers et al. (2009), Pietras et al. (2014), and Sato et al. (2009). While mice responded with blood cytopenia, thrombocytopenia, and bone marrow aplasia, only the bone marrow cellularity was more affected in *Nfat5*<sup>fl/fl</sup> LysM-Cre mice compared with wild-type mice (Fig. 4 C). Acute poly(I:C) treatment was then used as the model of systemic IFN-I-mediated HSC activation, which we measured by analyzing the percentage of bone marrow lineage<sup>-</sup> Sca-1<sup>+</sup> cKit<sup>+</sup> cells (LSK), HSCs (CD150<sup>+</sup> CD48<sup>-</sup> LSK), multipotent progenitors 3/4 (MPP3/4; CD150<sup>-</sup> CD48<sup>+</sup> LSK), and MPP2 (CD150<sup>+</sup> CD48<sup>+</sup> LSK). As expected from their elevated production of IFNα, we detected increased percentages of LSK, MPP3/4, MPP2, and HSC populations in the bone



**Figure 3. NFAT5 represses IFN-I responses in macrophages and DCs infected with different viruses.** (A and B) Expression of the mRNA of *Ifnb1* and ISGs *Ifit2* and *Mx1* in NFAT5-deficient (*Nfat5*<sup>-/-</sup>) and wild-type (*Nfat5*<sup>+/+</sup>) BMDMs (A) and BMDCs differentiated with GM-CSF (GM-BMDCs; B) at different times after infection with VSV (top) or MCMV (bottom), using a multiplicity of infection (MOI) of 1. mRNA values for each gene were normalized to L32 RNA and are represented as relative to the 12-h infection time point in wild-type cells. Expression of *Nfat5* mRNA in wild-type BMDMs is also shown ( $n = 4$ ). (C) Wild-type (*Nfat5*<sup>+/+</sup>) and NFAT5-deficient (*Nfat5*<sup>-/-</sup>) BMDCs differentiated with Flt3L and sorted as pDCs (CD11c<sup>+</sup> B220<sup>+</sup>) were infected with VSV (for 6 h; left) or LCMV (for 12 h; right) to analyze mRNA levels of *Ifnb1*, *Ifna1*, and *Ifna7*, and the ISG *Ifit2*. mRNA values for each gene were normalized to L32 RNA and are represented as relative to infected wild-type cells. (D) Expression levels of the mRNA of *Ifnb1*, *Ifna1*, and *Ifna7* in wild-type, NFAT5-deficient (*Nfat5*<sup>-/-</sup> Vav-Cre), IFNAR1-deficient (*Nfat5*<sup>+/+</sup> Vav-Cre *Ifnar1*<sup>-/-</sup>), or NFAT5- and IFNAR1-deficient (*Nfat5*<sup>-/-</sup> Vav-Cre, *Ifnar1*<sup>-/-</sup>) BMDMs at the indicated times after VSV infection at MOI 1. mRNA values for each gene were normalized to L32 RNA and are represented as relative to VSV-infected wild-type cells. (E) Expression of *Ifnb1* and *Ifit2* mRNA in *Nfat5*<sup>+/+</sup> and *Nfat5*<sup>-/-</sup> BMDMs 12 h after infection with UV-inactivated VSV. Error bars in A–E show the mean  $\pm$  SEM. Results in A and B are from three

independent experiments, each comparing cells from one NFAT5-deficient mouse and one wild-type littermate. Results in C comprise six BMDC cultures of each genotype for VSV and four for LCMV analyzed in four independent experiments. Results in D comprise six BMDM cultures of each genotype from three independent experiments. Results in E show the mean  $\pm$  SEM of five BMDM cultures of wild-type and NFAT5-deficient from three independent experiments. Statistical significance in A and B was determined with a one-sample *t* test for comparisons with the reference sample (wild-type cells infected for 12 h) or with an unpaired *t* test for comparisons between the other samples. Statistical significance in C was determined with a one-sample *t* test using infected wild-type cells as reference. Statistical significance in D and E was determined with an unpaired *t* test. \*, *P* < 0.05; \*\*, *P* < 0.01.

marrow of poly(I:C)-treated, NFAT5-deficient mice (Fig. 4, D and top graphs in E; and Fig. S3, A and B). As Sca-1, one of the markers generally used to identify hematopoietic progenitor populations, can be induced by IFN-I in other potentially contaminant cell types, we further confirmed the identity of HSCs by including the marker ESAM (Ooi et al., 2009; Pietras et al., 2014), which was highly expressed in HSCs of both mouse genotypes in basal and poly(I:C) treatment conditions (Fig. 4 E, middle graphs; and Fig. S3 A). We also observed that acute poly(I:C) treatment increased the percentage of apoptotic LSK, HSCs, and MPP3/4 cells in NFAT5-deficient, but not in wild-type, mice (Fig. 4 E, bottom graphs), and reduced their pool of quiescent (Ki67<sup>neg</sup>) HSCs (Fig. 4, F and G; and Fig. S3 C). Here, we noticed that loss of HSC quiescence in NFAT5-deficient mice occurred in their CD41<sup>neg</sup> subset (Fig. 4 G), which has been described to comprise mostly quiescent cells (Bernitz et al., 2016). Altogether, these results indicated that systemic acute IFN-I overproduction in NFAT5 mouse models caused exacerbated HSC activation and compromised viability of hematopoietic cell precursors. Increased systemic production of IFN-I in NFAT5-deficient mice caused enhanced IFNAR signaling in HSC precursors of these mice, evidenced by increased STAT1 phosphorylation, higher levels of the IFN-I-inducible receptor Sca-1, and higher expression of other ISGs (Fig. 4, H and I; and Fig. S3 D). In line with the idea that exacerbated HSC activation in NFAT5-deficient mice was caused by their increased production of IFN-I, treatment of wild-type and *Nfat5*<sup>fl/fl</sup> Vav-Cre mice with the same dose of IFN $\alpha$  (100,000 U/mice) induced the same extent of HSC activation and increased proportions of LSK and MPP3/4 in both types of mice (Fig. S3, E and F). Deletion of IFNAR rescued the proportions of quiescent HSCs in poly(I:C)-treated mice to the levels of untreated mice and also abrogated the differences between *Nfat5*<sup>fl/fl</sup> Vav-Cre and wild-type mice (Fig. 4 J), indicating that the main driver of HSC activation upon poly(I:C) treatment is IFN-I and supporting the role of NFAT5 in the control of systemic IFN-I-induced HSC activation.

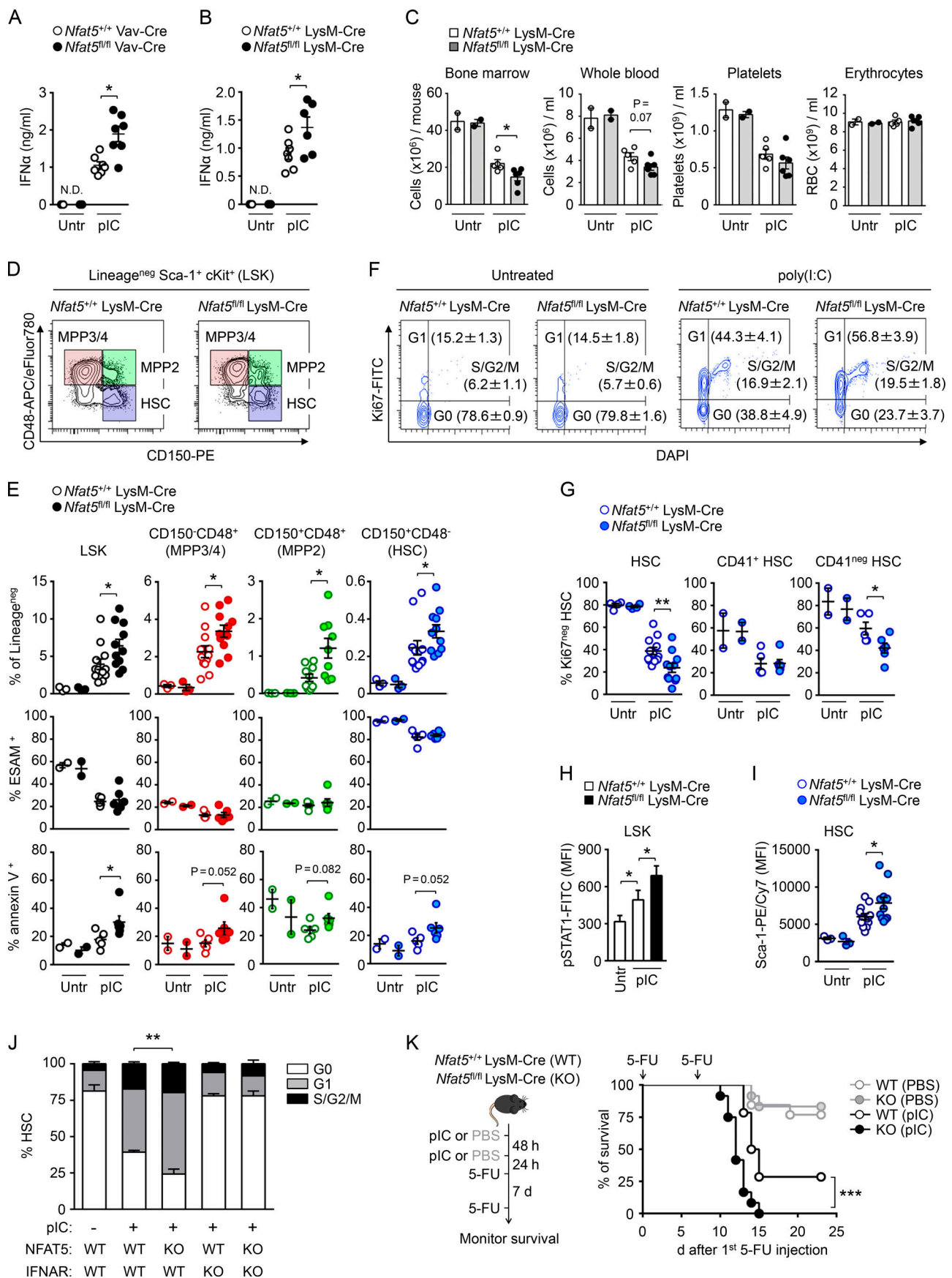
We next analyzed diverse hematological and hematopoietic parameters in the model of acute LCMV infection. We first conducted time course experiments in wild-type mice (Fig. S4, A–C) and chose day 3 after infection for further comparison with NFAT5-deficient mice. As shown above, acute LCMV infection induced lower systemic IFN-I production than poly(I:C) (compare wild-type mice in Fig. 2, A and E with Fig. 4, A and B), and, consistent with this, short-term responses to LCMV showed milder changes in bone marrow aplasia (compare wild-type mice in Fig. 4 C with Fig. S4 D). These parameters were largely similar in myeloid-specific NFAT5-deficient and control mice (Fig. S4, D and E), but

increased numbers of lineage-negative bone marrow cells and HSCs were detected in the infected NFAT5-deficient mice (Fig. S4 E, left). Although differences in hematopoietic progenitors between NFAT5-deficient and wild-type mice were more modest in the acute LCMV infection model, they were in line with the effect of poly(I:C) treatment. Cycling HSCs are sensitive to repetitive treatment with the chemotherapeutic drug 5-fluorouracil (5-FU; Lerner and Harrison, 1990). To test whether NFAT5-controlled IFN-I production is a relevant contributor to limit HSC activation, we primed myeloid-specific NFAT5-deficient and control mice with poly(I:C) and subjected them to two rounds of 5-FU treatment 7 d apart, as in Essers et al. (2009) (Fig. 4 K, left). As predicted from their reduced proportion of quiescent HSCs after poly(I:C) treatment (Fig. 4 G), primed *Nfat5*<sup>fl/fl</sup> LysM-Cre mice were more vulnerable to 5-FU-mediated toxicity than littermate controls (Fig. 4 K, right). Altogether, these findings indicate that NFAT5 limits systemic IFN-I production by diverse immune cells, and this preserves quiescence of HSCs.

#### NFAT5 binds to the *Ifnb1* promoter and limits recruitment of IRF3

Our previous results showed that NFAT5 repressed IFN-I expression induced by poly(I:C) and viruses, but not upon direct stimulation with IFN-I, and that lack of NFAT5 did not affect activation of the IFN-I master transcriptional regulator IRF3. These observations suggested that NFAT5 might act by targeting IFN-I genes. We first confirmed that the ability of NFAT5 to limit IFN-I induction required its direct binding to DNA. For this, we took advantage of NFAT5-deficient MEFs, which express a shorter form of NFAT5 with an internal deletion that eliminates the first exon of its Rel-like DNA binding domain (DBD), and therefore lacks DNA binding capacity but preserves its dimerization domain and the long C-terminal region ( $\Delta$ DBD NFAT5; Fig. 5, A and B; López-Rodríguez et al., 2004; Stroud et al., 2002). We observed enhanced induction of *Ifnb1* and *Ifit2* genes in VSV-infected, NFAT5-deficient MEFs ( $\Delta$ DBD NFAT5; Fig. 5 C), indicating that the inhibitory control of NFAT5 in the IFN-I pathway was mediated by the ability to contact its specific target sites in DNA. As an approach to identify NFAT5-binding sites in regulatory regions of IFN-I genes, we performed whole genome ultrasequencing of NFAT5-immunoprecipitated chromatin (ChIP) using unstimulated and poly(I:C)-treated wild-type and NFAT5-deficient macrophages. We did not detect significant NFAT5 binding peaks in a broad region spanning the IFN-I locus in mouse chromosome 4 (not shown). This region included various *Ifna* genes and *Ifnb1*. As the *Ifnb1* promoter contains a clear consensus binding site for NFAT5 (5'-AG-GAAAA-3'), for which we already had evidence of NFAT5



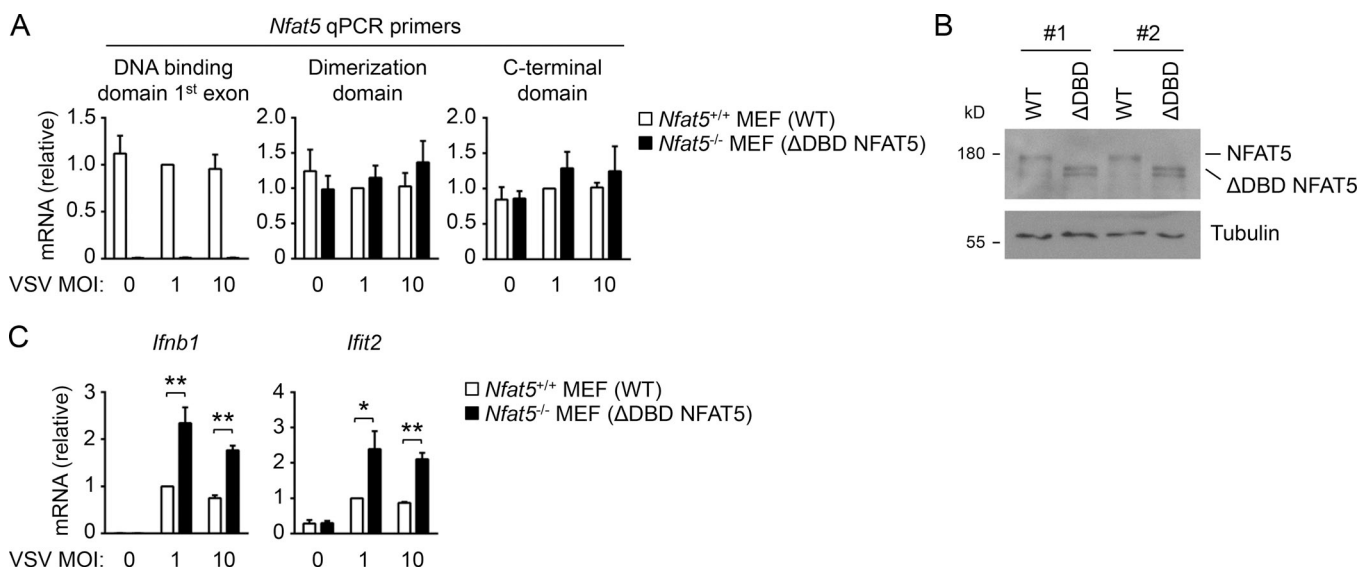


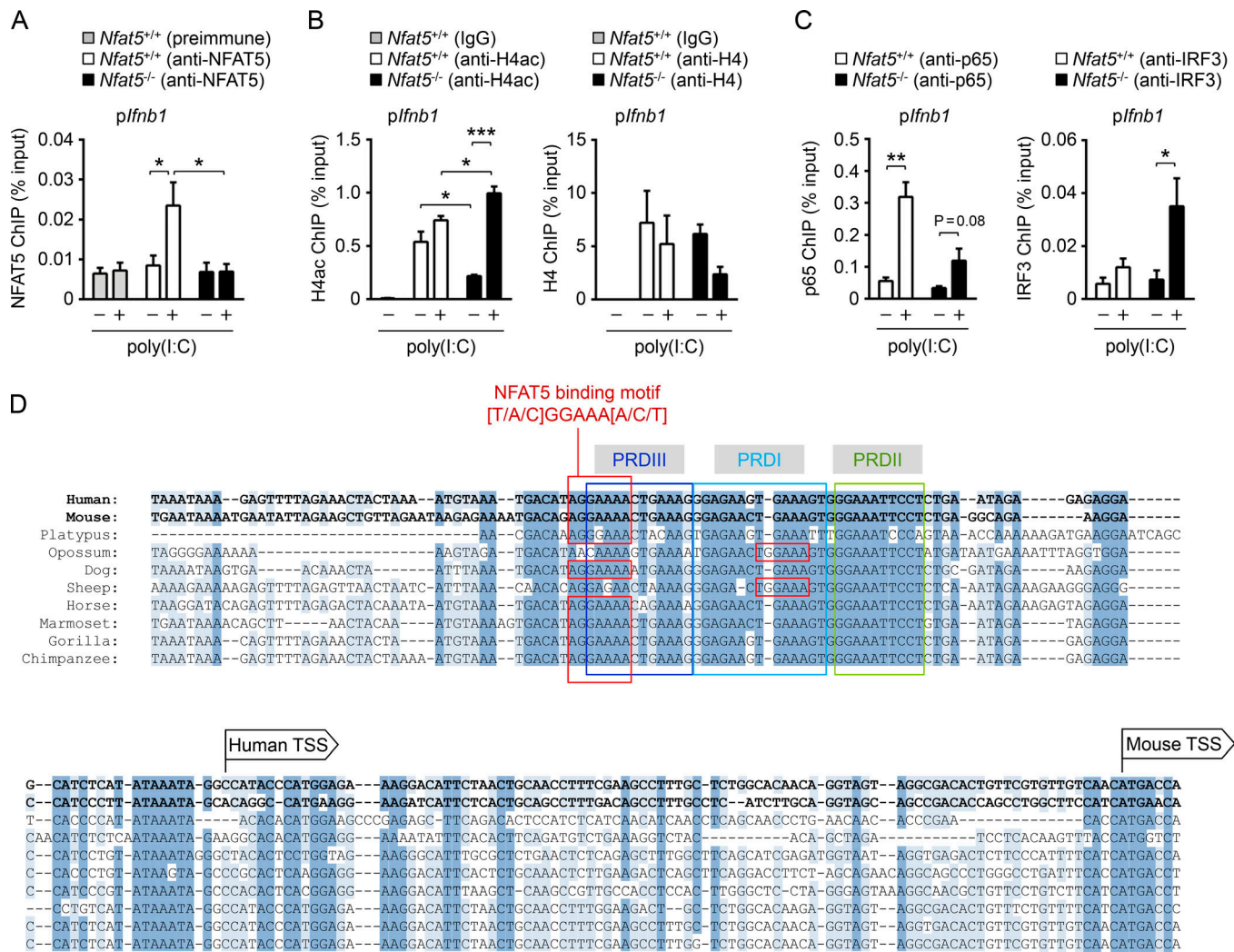


**Figure 4. Exacerbated IFN-I response in NFAT5-deficient mouse models causes enhanced activation of HSCs.** (A and B) IFN $\alpha$  levels in serum of untreated (Untr,  $n = 3$ ) or poly(I:C)-treated ( $n = 6-7$ ) mice (pIC; 2.5 mg/kg, 12 h) were measured by ELISA in wild-type and *Nfat5<sup>fl/fl</sup>* Vav-Cre (A) or *Nfat5<sup>fl/fl</sup>* LysM-Cre mice (B). Results (mean  $\pm$  SEM) in A and B are from two independent experiments. N.D., not detected. (C) Number of cells, platelets, and erythrocytes in whole blood and bone marrow cellularity in wild-type and *Nfat5<sup>fl/fl</sup>* LysM-Cre mice left untreated or treated with poly(I:C) (two doses of 2.5 mg/kg of poly(I:C) administered 48 h apart and analyzed 24 h after the second injection). Bone marrow cell numbers were counted from two femurs and two tibiae per mouse. Results (mean  $\pm$  SEM) are from one experiment with five treated and two untreated mice of each genotype. (D) Panels show representative flow cytometry analysis of hematopoietic progenitor and stem cells within LSK cells in the bone marrow of *Nfat5<sup>+/+</sup>* LysM-Cre and *Nfat5<sup>fl/fl</sup>* LysM-Cre mice treated with poly(I:C) as in C. The gating strategy is shown in Fig. S3 A. (E) The upper panels show the percentages of LSK and the indicated populations within LSK cells in untreated and poly(I:C)-treated mice, the middle panels show the percentage of ESAM<sup>+</sup> cells in the different subsets, and the bottom panels show the percentage of annexin V<sup>+</sup> cells in the indicated subsets. Solid dots represent individual NFAT5-deficient mice, and empty dots are wild-type mice. (F) Representative contour plots for cell cycle analysis in HSCs in G. (G) Percentage of quiescent (Ki67<sup>neg</sup>) HSCs and their CD41<sup>+</sup> and CD41<sup>neg</sup> subsets in wild-type and NFAT5-deficient mice treated as in C. (H) Phospho-STAT1 (Y701) levels measured by intracellular staining and flow cytometry in LSK cells of untreated *Nfat5<sup>+/+</sup>* Vav-Cre (wild-type) mice ( $n = 3$ ), and poly(I:C)-treated (2.5 mg/kg, 16 h) *Nfat5<sup>+/+</sup>* Vav-Cre ( $n = 4$ ) and *Nfat5<sup>fl/fl</sup>* Vav-Cre ( $n = 4$ ) mice. MFI, median fluorescence intensity. (I) Sca-1 levels measured by flow cytometry in HSCs from top panel in E. Error bars in E and G–I show the mean  $\pm$  SEM. Results for hematopoietic subsets analysis in E, Ki67 analysis in whole HSCs in G, and Sca-1 MFI in I are from two independent experiments, with a total of 3–4 untreated mice of each genotype, 12 poly(I:C)-treated *Nfat5<sup>+/+</sup>* LysM-Cre mice, and 11 poly(I:C)-treated *Nfat5<sup>fl/fl</sup>* LysM-Cre mice. Results for ESAM, annexin V, and CD41 analyses in E and G are from one experiment with two untreated mice of each genotype, and five wild-type and six NFAT5-deficient poly(I:C)-treated mice. Results for phospho-STAT1 in H are from two independent experiments. (J) Percentage of HSCs in the indicated cell cycle phases after poly(I:C) treatment as in C in wild-type (three untreated, six treated), NFAT5-deficient (*Nfat5<sup>fl/fl</sup>* Vav-Cre,  $n = 4$ ), IFNAR-deficient (*Nfat5<sup>+/+</sup>* Vav-Cre, *Ifnar1<sup>-/-</sup>*,  $n = 6$ ), or NFAT5- and IFNAR-deficient mice (*Nfat5<sup>fl/fl</sup>* Vav-Cre, *Ifnar1<sup>-/-</sup>*,  $n = 4$ ). Results (mean  $\pm$  SEM) are from four independent experiments with one to two mice of each genotype per condition and experiment. Statistical significance in A–J was determined with an unpaired *t* test. \*,  $P < 0.05$ ; \*\*,  $P < 0.01$ . \*\* in J is for the difference between wild-type and NFAT5-deficient HSCs in the percentage of cells in G0 and G1 upon poly(I:C) treatment in vivo. (K) Schematic diagram of the poly(I:C) conditioning and 5-FU challenge experiment (left), and Kaplan-Meier representation (right) of survival of *Nfat5<sup>+/+</sup>* LysM-Cre (WT) and *Nfat5<sup>fl/fl</sup>* LysM-Cre (KO) mice under this protocol (13 WT mice treated with 5-FU without poly(I:C) conditioning, 14 WT mice treated with 5-FU after poly(I:C), 12 knockout mice treated with 5-FU without poly(I:C), and 12 knockout mice treated with 5-FU after poly(I:C)). Results are from two independent experiments. Statistical significance in K was determined with a Mantel-Cox test. \*\*\*,  $P < 0.001$ .

recruitment (see below), we suspected that the ChIP-sequencing assay was not sufficiently sensitive to detect some NFAT5-bound regions, as we had already noticed in a recent work (Buxadé et al., 2018).

We then assessed the binding of NFAT5 to the promoter of *Ifnb1* by quantitative ChIP (qChIP) in poly(I:C)-treated BMDMs. We used the preimmune sera and NFAT5-deficient cells as controls for specificity of the NFAT5 ChIP. These experiments





**Figure 6. NFAT5 binds to the *Ifnb1* promoter and limits recruitment of IRF3.** (A) ChIP and quantitative PCR (qChIP) analysis of NFAT5 binding to the *Ifnb1* promoter in NFAT5-deficient (*Nfat5*<sup>-/-</sup>) and wild-type (*Nfat5*<sup>+/+</sup>) BMDMs left untreated (-) or stimulated with poly(I:C) (+; 1 µg/ml, 2.5 h). (B) qChIP analysis of H4ac and total H4 in the *Ifnb1* promoter in untreated or poly(I:C)-treated *Nfat5*<sup>-/-</sup> and *Nfat5*<sup>+/+</sup> BMDMs. (C) qChIP analysis of p65 and IRF3 recruitment to the *Ifnb1* promoter in untreated or poly(I:C)-treated *Nfat5*<sup>-/-</sup> and *Nfat5*<sup>+/+</sup> BMDMs. Results show the mean ± SEM of six BMDM cultures of each genotype analyzed in four independent experiments in A; three independent experiments in B, each with cells from one NFAT5-deficient mouse and one wild-type littermate; and five to six BMDM cultures of each genotype analyzed in C from three independent (p65) and four independent (IRF3) experiments. Statistical significance was determined with an unpaired t test. \*, P < 0.05; \*\*, P < 0.01; \*\*\*, P < 0.001. (D) Alignment of the *IFNB1* gene promoter regions in different mammalian species. Alignment of the indicated genomic regions was done with Jalview. The positions of IRF-binding sites PRDIII and PRDI and the NF-κB-binding site PRDII are marked with colored boxes. The NFAT5 consensus binding motif is shown in red letters. The position of a conserved NFAT5 consensus binding site that partially overlaps with PRDIII is indicated with red boxes. The NFAT5-binding site in PRDIII is lost in opossum and sheep but is found further downstream in PRDI (5'-TGGAAA-3'; marked with small red boxes). The transcription start sites (TSS) in human and mouse genomes are indicated. The position of the TSS in human *IFNB1* in current databases has been updated with respect to the position originally used in the *IFNB1* promoter reporter in Fig. 7.

showed that NFAT5 was recruited to *Ifnb1* promoter in response to poly(I:C) stimulation (Fig. 6 A). Since the *Ifnb1* promoter is centrally regulated by recruitment of transcription factors p65/NF-κB and IRF3 and histone acetylation (Agalioti et al., 2000; Honda et al., 2006), we asked whether these parameters were altered in NFAT5-deficient macrophages. NFAT5-deficient cells had lower levels of acetylated histone H4 (H4ac) than wild-type cells in the *Ifnb1* promoter in unstimulated conditions but increased them upon poly(I:C) stimulation above the levels of wild-type cells (Fig. 6 B). We also found that NFAT5-deficient BMDMs showed reduced p65/NF-κB recruitment but enhanced

IRF3 recruitment to the *Ifnb1* promoter upon poly(I:C) stimulation (Fig. 6 C). Our finding of enhanced IRF3 recruitment to the *Ifnb1* promoter in NFAT5-deficient cells paralleled by increased H4ac levels is consistent with earlier works showing that IRF3 reduces histone density and enhances histone acetylation in the *Ifnb1* promoter upon stimulation (Sato et al., 1998; Yoneyama et al., 1998; Agalioti et al., 2000). Altogether, our results suggested that *Ifnb1* transcription in NFAT5-deficient macrophages became mainly controlled by IRF3 rather than NF-κB, and indicated that binding of IRF3 to the *Ifnb1* promoter could be a central target of the inhibitory function of NFAT5.

### Repression of the *IFNB1* promoter by NFAT5 is mediated by an evolutionarily conserved NFAT-IRF overlapping site

The core structure of elements regulating *Ifnb1* expression is well conserved between the proximal mouse and human gene promoters, and indeed this homology extends to the genomes of other mammal species (Fig. 6 D). Elements displaying a strong degree of conservation across multiple species include the sites bound by IRF (PRDIII and PRDI) and NF- $\kappa$ B (PRDII) transcription factors (Honda et al., 2006; Levy et al., 2011; Panne et al., 2007), and also a clear NFAT5-binding consensus (5'-AGGAAAA-3') that partly overlaps with the IRF site in PRDIII (Fig. 6 D). We therefore used a reporter of the minimal human IFN $\beta$  promoter (*IFNB1*-Luc) to ask whether the activity of this region was under the control of NFAT5. We observed that inhibition of NFAT5 expression (shNFAT5; Fig. 7 C) doubled the poly(I:C)-induced activation of the *IFNB1*-Luc reporter (Fig. 7 A, left panel), indicating that this short region of the *IFNB1* promoter was the target of NFAT5. In this regard, and also in line with our observations with  $\Delta$ DBD NFAT5 MEFs (Fig. 5), overexpression of the isolated NFAT5-DBD (López-Rodríguez et al., 2001) reduced the activity of the *IFNB1* promoter (Fig. 7 A, right), again indicating that NFAT5 limited *IFNB1* transcription through its ability to bind DNA. Reporters driven by specific IRF or NF- $\kappa$ B elements in the *IFNB1* promoter (3 $\times$  PRDIII-I or 2 $\times$  PRDII, respectively; Escalante et al., 2002, 2007) showed that suppressing NFAT5 significantly increased the poly(I:C)-induced activity of the IRF-regulated 3 $\times$  PRDIII-I, but not that of the NF- $\kappa$ B-regulated 2 $\times$  PRDII (Fig. 7 B). This finding pointed to IRF elements as the target of the inhibitory control of NFAT5. Seeing that there is a consensus NFAT5-binding sequence partially overlapping the key IRF-binding site of PRDIII (Fig. 6 D), one possibility consistent with our qChIP results (Fig. 6, A–C) is that binding of NFAT5 to this region of the *IFNB1* promoter could limit the accessibility of IRF3, the master regulator of IFN-I expression. We therefore introduced mutations in *IFNB1*-Luc that specifically targeted nucleotides required for NFAT5, IRF, or NF- $\kappa$ B binding (Fig. 7 D). While disrupting the NFAT5 site (Lopez-Rodríguez et al., 1999; -91G $\rightarrow$ A) nearly doubled the poly(I:C)-induced activity of this reporter, mutation of either of the two IRF-binding sites (-83GA $\rightarrow$ CT in PRDIII or -70GA $\rightarrow$ CT in PRDI) or the NF- $\kappa$ B binding element (-56CC $\rightarrow$ TT in PRDII; Escalante et al., 2002, 2007) impaired its activation (Fig. 7 E). This effect was quite pronounced for the PRDIII mutation, which lost responsiveness to poly(I:C), highlighting the central role of this element in the control of *IFNB1*. We also verified that mutation of the NFAT5 site (-91G $\rightarrow$ A) rendered the *IFNB1*-Luc reporter insensitive to overactivation by shNFAT5 (Fig. 7 F), indicating that this was the DNA element mediating the inhibitory effect of NFAT5. In this regard, while mutation of the consensus binding site of NFAT5 could increase the residual poly(I:C)-induced activity of the reporters carrying the PRDI or the PRDII mutants, it did not rescue any activity from the PRDIII mutant (Fig. 7 G), further supporting that partial overlap between the IRF and NFAT5 sites in PRDIII could be the mechanism that balances IFN $\beta$  expression. By contrast, the role of NF- $\kappa$ B in the regulation of *IFNB1* transcription was disconnected from the NFAT5-IRF competition as its mutant not only conserved responsiveness of the *IFNB1* promoter to poly(I:C), but

also its NFAT5-dependent repression (Fig. 7 G, right). These reporter assays are consistent with the result that enhanced IRF3 recruitment to the *Ifnb1* promoter in NFAT5-deficient macrophages sufficed to increase IFN $\beta$  expression despite reduced binding of p65. Altogether, analysis of the mechanism by which NFAT5-deficient cells enhance IFN $\beta$  expression indicates that they use a transcription factor complex whose components differ from those used by wild-type cells.

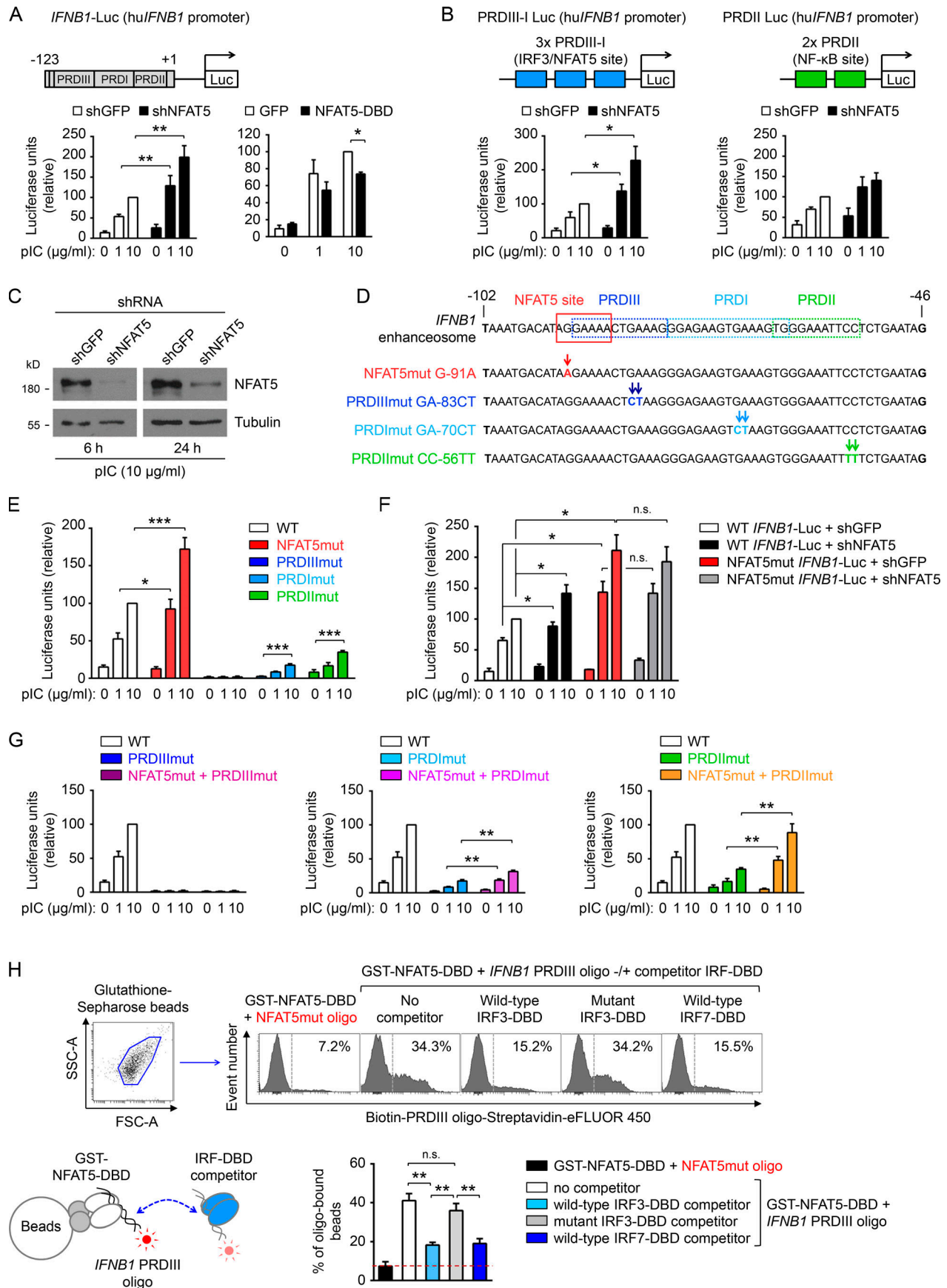
Our findings with the different PRDIII mutants point to a competition between IRF3 and NFAT5 for binding to this element. We addressed this possibility using a cell-free protein-DNA binding assay (Fig. 7 H). First, we confirmed the direct binding of NFAT5-DBD to a PRDIII oligonucleotide probe, but not to a probe mutated in the key NFAT5 site required for repression of the *IFNB1* promoter (-91G $\rightarrow$ A; Fig. 7, D, E, and H). Binding of NFAT5 to PRDIII was inhibited by the DBD of IRF3 and IRF7, but not by a mutant IRF3 DBD that does not bind DNA (Fig. 7 H; Escalante et al., 2007). Together with our previous results, the experiments showing that NFAT5 and IRFs can displace each other at the PRDIII element illustrate a mechanism at the genomic level that limits *IFNB1* transcription through a dual NFAT5-IRF-controlled site embedded in its enhanceosome.

## Discussion

Here, we show that the transcription factor NFAT5, an inducer of inflammatory responses in macrophages, is also a repressor of IFN-I expression. We found that a key IRF3-dependent activator element in the *IFNB1* enhanceosome contains an overlapping binding site for NFAT5, which opposes IRF3 and thus balances IFN $\beta$  expression. This genomic arrangement has been maintained through the evolution of mammals, yet the existence of a hidden NFAT5-negative regulatory element within was not suspected. Our results show that the opposition between NFAT5 and IRF3 in the *IFNB1* enhanceosome controls the expression of IFN-Is and their ISG targets in different types of cells. NFAT5 limits the magnitude of IFN-I response in vivo and has a significant impact on both antiviral defense and maintenance of HSC quiescence.

NFAT5 occupies a distinct functional niche in the control of antipathogen responses by attenuating IFN-I gene induction while enhancing expression of other inflammatory mediators (Buxadé et al., 2012; Tellechea et al., 2018). This unique duality is the result of the mechanism through which NFAT5 inhibits IFN-I expression by opposing IRF3, the master transcription factor specialized in IFN-I expression. This mode of action differs from known factors that attenuate IFN-I expression. ATF3 is considered a general repressor of macrophage inflammatory responses, as it not only inhibits *Ifnb1* transcription but also multiple other inflammatory genes, including *Nos2*, *Tnf*, *Il6*, and *Il12b* (Labzin et al., 2015; Gilchrist et al., 2006). IRF2 represses IFN-I in virus-infected fibroblasts by preventing the recruitment of transcription coactivators to the *IFNB1* enhanceosome (Matsuyama et al., 1993; Senger et al., 2000), but then it promotes TLR3 expression in macrophages so that the net effect of IRF2 in poly(I:C)-stimulated macrophages is to enhance IFN $\beta$  production (Nhu et al., 2006). Unlike ATF3, NFAT5 is not a





**Figure 7. Repression of the *IFNB1* promoter by NFAT5 is mediated by an overlapping NFAT-IRF site.** (A) Activity of a luciferase reporter driven by the human *IFNB1* promoter (*IFNB1*-Luc) in unstimulated or poly(I:C)-stimulated (6 h) RAW 264.7 macrophage cells transfected with shNFAT5 or shGFP (left), or with plasmids encoding the DBD of NFAT5 fused to GFP (NFAT5-DBD) or GFP alone (right). (B) Activity of the 3× PRDIII-I Luc (left) and 2× PRDII-Luc (right) reporters in unstimulated or poly(I:C)-stimulated (6 h) RAW 264.7 cells transfected with shNFAT5 or shGFP. (C) Western blot of NFAT5 in poly(I:C)-treated RAW 264.7 cells transfected with shGFP or shNFAT5. (D) Mutagenesis strategy to target the consensus binding sites for NFAT5, IRF3 (PRDIII and PRDI), and NF-κB (PRDII) in the *IFNB1* enhanceosome. (E–G) Activity of the corresponding *IFNB1*-Luc reporter mutants. In all experiments, luciferase activity was normalized for the efficiency of electroporation using a Renilla-expressing plasmid cotransfected in the same cells. Normalized luciferase units in each experiment are shown relative to a reference sample (with value 100) of cells transfected with control shGFP plasmid or GFP-encoding plasmid and stimulated with 10 μg/ml poly(I:C). Error bars in A, B, and E–G show the mean ± SEM. Results in A are from 10 independent transfection experiments in the left panel and 3 in the right panel. Results in B are from six independent transfection experiments in the left panel and four in the right panel. Western blots in C are representative of two independent experiments. Results in E and G are from six independent transfection experiments and from three independent experiments in F. Statistical significance was determined with a one-sample *t* test for comparisons with the reference sample or with an unpaired *t* test for comparisons between the other samples. \*, *P* < 0.05; \*\*, *P* < 0.01; \*\*\*, *P* < 0.001. (H) Flow cytometry assay to assess the competition between the DBDs of NFAT5 and IRF proteins at the PRDIII element of the *IFNB1* enhanceosome. The schematic diagram depicts a GST-tagged DBD of NFAT5 (GST–NFAT5-DBD) bound to a biotin-tagged, double-strand PRDIII oligonucleotide (*IFNB1* PRDIII oligo) and captured on glutathione-Sepharose beads. The *IFNB1* PRDIII oligo is detected by flow cytometry with eFluor 450–labeled streptavidin. Competition between IRF and NFAT5 was assessed by preincubating the *IFNB1* PRDIII oligo with recombinant IRF-DBD. The flow cytometry dot plot shows the forward scatter (FSC) and side scatter (SSC) profiles in logarithmic scale (log10) of the glutathione-Sepharose beads, and the histograms on the right show the eFluor 450 signal on NFAT5-coated beads for a mutant *IFNB1* PRDIII oligo with the NFAT5 site disrupted (NFAT5mut oligo, used to determine the nonspecific binding background), and for the wild-type *IFNB1* PRDIII oligo in the absence or presence of competitor IRF3 (wild-type and DNA binding mutant) and IRF7. The bars show the quantification of the flow cytometry assays. Results are from two independent experiments, each one with two technical replicates for each binding reaction. Statistical significance was determined with an unpaired *t* test. \*\*, *P* < 0.01.

general inhibitor of inflammatory genes, as it enhances TLR-induced expression of pro-inflammatory genes unrelated to IFN-I, such as *Nos2*, *Tnf*, *Il6*, and *Il12b* (Buxadé et al., 2012; Tellechea et al., 2018), and in contrast to IRF2, NFAT5 represses *Ifnb1* in fibroblasts as well as in macrophages and DCs, both in response to viral infection and TLR3 stimulation without affecting TLR3 expression.

Our results point to an evolutionarily conserved mechanism by which NFAT5 could limit IFN-I responses by attenuating the expression of both IFNβ and IFNα. IFNβ is a main point of control of the IFN-I pathway in macrophages and myeloid DCs due to its ability to enhance expression of several IFNα forms through a positive feedback via IFNAR signaling and induction of IRF7 (Honda and Taniguchi, 2006; Marié et al., 1998). Our finding that IFNβ is a direct target repressed by NFAT5 in macrophages suggests that the impact of NFAT5 on IFNα could be a consequence of its primary effect on IFNβ. This reasoning is also supported by our finding that NFAT5 did not affect the magnitude of *Ifna1* and *Ifna7* induction when macrophages were stimulated with exogenous IFNα or IFNβ instead of TLR ligands. However, we also observed that lack of NFAT5 caused a mild increase in the short-term induction of *Ifna1* during VSV infection in IFNAR-deficient macrophages, which would be independent of prior IFNβ signaling. This observation raises the question of whether NFAT5 might directly repress the expression of some *Ifna* genes in specific stimulatory contexts. In this regard, and similarly to what we have observed in the *IFNB1* promoter (Fig. 6 D), we noticed that the virus-responsive elements of genes encoding for several IFNα forms in humans and mice (Chen et al., 2004; van Pesch et al., 2004) contain an NFAT5 consensus motif (5'-T/AGGAAA-3'; Lopez-Rodríguez et al., 1999) overlapping IRF-binding sites. Also, while induction of IFNα in macrophages and myeloid DCs depends on IFNβ-mediated activation of IRF7, pDCs express IRF7 constitutively (Honda et al., 2005), and this allows them to produce IFNα independently of IFNAR feedback (Barchet et al., 2002). Our

finding that NFAT5-deficient pDCs expressed three- to fivefold more *Ifnb1*, *Ifna1*, and *Ifna7* than wild-type cells upon viral infection suggests the possibility, supported by our in vitro competition assays, that NFAT5 could also regulate expression of diverse IFN-I by opposing IRF7.

While our results show that NFAT5 opposes IRFs and attenuates IFN-I induction in macrophages and DCs, a recent work has shown that the calcineurin-activated NFATC3 enhances the IRF7-dependent activation of *Ifnb1* and *Ifna4* promoters in pDCs (Bao et al., 2016). Bao et al. (2016) also found that deletion of NFATC3 in human pDCs partially impaired the recruitment of IRF7 to the *Ifnb1* promoter and showed that NFATC3 could bind an *Ifnb1* promoter oligonucleotide spanning the PRDIII, I, and II motifs that contains the GGAAA NFAT-binding site. These findings and our results suggest that IFN-I production in pDCs could be regulated under different stimulatory inputs through a balance between NFAT5 and NFATC3 and their respective abilities to oppose or cooperate with IRF proteins. While both NFAT5 and NFATC3 recognize GGAAA elements, NFAT5 differs from calcineurin-regulated NFATC factors in that it binds DNA as a constitutive dimer that encircles its target site, whereas NFATC proteins bind DNA as monomers and can partner with Fos and Jun proteins, which NFAT5 does not (Lopez-Rodríguez et al., 1999; López-Rodríguez et al., 2001; Stroud et al., 2002). It is possible that the bulkier NFAT5 dimer could hinder the recruitment of IRFs to the PRDIII element whereas monomeric NFATC3 would permit it and even favor it. This possibility could be assessed through structural analysis and modeling the effect of NFAT5 and NFATC3 on the binding of IRFs to the PRDIII site. Finally, another implication of the NFAT5-IRF competition mechanism is that IRF target genes whose promoters lacked a specific configuration of overlapping NFAT5-IRF sites would not be repressed by NFAT5. Further research will be needed to test this possibility by identifying IRF3-dependent genes repressed or unaffected by NFAT5.

The functional significance of NFAT5-mediated IFN-I repression connects with its role as inducer of pro-inflammatory and antipathogen gene expression downstream PRRs (Buxadé et al., 2012; Tellechea et al., 2018). While evidently playing a protective role against viruses, IFN-I produced in antiviral responses can weaken other antipathogenic defenses and make the organism vulnerable to bacteria and fungi (Guarda et al., 2011; Shahangian et al., 2009). One mechanism by which IFN-I does so is by dampening production of inflammatory cytokines such as IL-1 $\beta$  in macrophages (Guarda et al., 2011). NFAT5 can enhance specific antipathogenic responses in TLR-activated macrophages by promoting expression of pro-inflammatory genes including *Il1b* (Buxadé et al., 2012; Tellechea et al., 2018), and this capacity could be modulated by its ability to repress IFN-I. Elucidating how NFAT5 affects the interplay between inflammatory and IFN-I responses during overlapping viral and bacterial infections is an open question for future studies.

While NFAT5-mediated attenuation of IFN-I could reduce the strength of antiviral responses in the short term, it also helped maintain HSC quiescence and viability during acute poly(I:C) treatment. Persistent IFN-I production can lead to exhaustion of hematopoietic progenitor pools, induce apoptosis in proliferating HSCs, and promote immunomodulatory mechanisms that inhibit effector T cell responses in chronic infections (Essers et al., 2009; Pietras et al., 2014; Ng et al., 2013; Teijaro et al., 2013). Our results suggest the possibility, which remains to be explored, that the ability of NFAT5 to reduce IFN-I production could confer long-term benefits by lessening these detrimental effects. Ultimately, the ability of NFAT5 to enhance or repress different antipathogen responses connects with the notion that the immune system has been tuned through evolution to safely balance effectiveness of antipathogen responses against their potential harmful effects to the organism.

## Materials and methods

### Mice

*Nfat5*<sup>+/-</sup> heterozygous mice in a pure 129/sv background were crossed to obtain *Nfat5*<sup>-/-</sup> and *Nfat5*<sup>+/+</sup> littermates as described (Buxadé et al., 2012). *Nfat5*-floxed (*Nfat5*<sup>fl/fl</sup>) mice in a pure C57BL/6 background were crossed with LysM-Cre mice to obtain mice lacking *Nfat5* in myeloid cells, and with Vav-Cre mice to obtain mice lacking NFAT5 in immune cell lineages (Buxadé et al., 2018). LysM-Cre mice were purchased from The Jackson Laboratory (Cat# 004781), and Vav-Cre mice were kindly provided by Dr. Thomas Graf (Center for Genomic Regulation, Barcelona, Spain). *Ifnar*<sup>-/-</sup> mice were kept in C57BL/6 background and were obtained from Manuel Rebelo at the Rodent Facility of the Gulbenkian Institute (Lisbon, Portugal). Mice were housed in groups of two to five per cage, containing individuals of different genotypes, and they were analyzed between 8 and 16 wk of age. Mice were of the same sex in each individual experiment, and results were reproduced in independent experiments using either female or male mice without noticeable differences due to gender. Mice were bred and maintained in specific pathogen-free conditions, and animal handling and experiments were in accordance with protocols

approved by the ethics committee of the Barcelona Biomedical Research Park/Universitat Pompeu Fabra Animal Care and Use Committee, and performed in accordance with the Declaration of Helsinki and the European Communities Council Directive (86/609/EEC).

### In vivo LCMV infection

8–12-wk-old mice were infected i.p. with a low dose ( $2 \times 10^2$  PFUs) of the strain Docile of LCMV to induce an acute infection. Mice were maintained under specific pathogen-free conditions in our in-house facility. Viral titers from the spleens of infected mice were determined on MC57 cells using the focus-forming assay as previously described (Battegay et al., 1991). A small piece of spleen was collected the day of necropsy and put directly at  $-80^\circ\text{C}$  until its use. For the assay, frozen spleens were smashed, resuspended in DMEM, and serial dilutions were made. Then, 200  $\mu\text{l}$  of the last three dilutions were placed in a 24-well plate containing 400,000 cells and incubated for 4 h at  $37^\circ\text{C}$ . Once the cells formed a monolayer, a 1:1 mixture of 3% methocel and  $2\times$  DMEM was added into each well and incubated at  $37^\circ\text{C}$  for 48 h. For the staining of PFUs, cells were fixed with 37% formaldehyde, washed twice with PBS, and incubated for 20 min with 1% Triton X-100 (TX-100) solution. For blocking nonspecific binding, cells were incubated for 1 h at room temperature with PBS containing 10% FCS. Cells were then incubated for 1 h with rat anti-LCMV nucleoprotein antibody VL-4 (Battegay et al., 1991) and for 1 h with anti-rat IgG HRP secondary antibody (Jackson ImmunoResearch, Cat# 112-035-003). To visualize the plaques, DAB Peroxidase Substrate kit (Vector Laboratories, Cat# SK-4100) was used.

### In vivo HSC activation and 5-FU challenge

To analyze HSC activation, 8–12-wk-old mice were injected i.p. with 2.5 mg/kg of poly(I:C) two times, 48 h apart, and analyzed 24 h after the second injection as described previously (Pietras et al., 2014). Fig. 4, D and F; and Figs. S2, A and B; and S3 A show the flow cytometry gating strategy for the analysis of diverse HSPC populations and analysis of Ki67/DAPI staining in HSCs (Sca-1<sup>+</sup> cKit<sup>+</sup> CD48<sup>-</sup> CD150<sup>+</sup>). 5-FU challenge was performed by i.p. injections of 150 mg/kg 5-FU at days 1 and 7 after the poly(I:C) injection, as shown in Fig. 4 K. Activation of HSCs with IFN $\alpha$  in vivo (24 h) was done by injecting IFN $\alpha$  (100,000 U/mouse; Miltenyi Biotec, Cat#130-093-131) subcutaneously as previously described (Essers et al., 2009).

### Analysis of hematological parameters

Peripheral blood (150  $\mu\text{l}$ ) from the tail vein was collected in EDTA-coated vials (Microvette; Sarstedt AG & Co., Cat# 20.1288). Blood hematological parameters were measured using a CVM-Procell hematology blood analyzer.

### Cells and viruses

BMDMs were generated as previously described (Buxadé et al., 2012). Briefly, mice were sacrificed and the femoral and tibial marrow was flushed from the bone with DMEM supplemented with 2 mM glutamine, 50  $\mu\text{M}$   $\beta$ -mercaptoethanol, and 1 mM sodium pyruvate plus penicillin/streptomycin (incomplete



medium). Cells were then resuspended in complete DMEM (incomplete medium supplemented with 10% heat inactivated FBS) with 25% (volume/volume) L929 supernatant (as the source of macrophage-CSF) and incubated for 6–7 d in polystyrene dishes at 37°C in 5% CO<sub>2</sub> atmosphere. For functional assays, BMDMs were harvested with PBS plus 5 mM EDTA by gentle pipetting, washed with PBS, and plated (10<sup>6</sup> cells/3 ml/well) in tissue culture plates. BMDCs were obtained by culturing bone marrow cell suspensions in 10% GM-CSF-supplemented medium for 10 d (Buxadé et al., 2018). In addition, Flt3L-induced conventional and pDCs were generated by culturing bone marrow cell suspensions in 200 ng/ml Flt3L (ImmunoTools, Cat# 12343305) for 10 d, after which BMDCs were isolated by flow cytometry cell sorting into CD11c<sup>+</sup> B220<sup>−</sup> (conventional BMDCs) and CD11c<sup>+</sup> B220<sup>+</sup> (plasmacytoid BMDCs). Peritoneal macrophages were harvested by two consecutive peritoneal lavages with 5 ml of ice-cold PBS and then isolated with magnetic beads coated with anti-CD11b antibody (M1/70.15 hybridoma supernatant; kindly provided by Dr. Gabriel Gil, Institut Hospital del Mar d'Investigacions Mèdiques, Barcelona, Spain). pDCs from spleens (CD11c<sup>+</sup> B220<sup>+</sup>) were obtained by flow cytometry cell sorting excluding dead cells (DAPI<sup>+</sup>) and neutrophils (Ly6G<sup>+</sup>). pDCs (DAPI<sup>−</sup> Ly6G<sup>−</sup> CD11c<sup>+</sup> B220<sup>+</sup>) and macrophages (DAPI<sup>−</sup> Ly6G<sup>−</sup> CD11b<sup>+</sup> F4/80<sup>+</sup>) were also obtained from bone marrow by flow cytometry cell sorting. HSCs were obtained from the bone marrow by flow cytometry cell sorting after lineage exclusion with antibodies against TER119, CD3, B220, CD11b, and Ly6G, and selection of Sca-1<sup>+</sup> cKit<sup>+</sup> CD48<sup>−</sup> CD150<sup>+</sup> cells. Gating strategies for flow cytometry and cell sorting are shown in Figs. S2, A and B, and S3 A. Primary MEFs from *Nfat5*<sup>+/+</sup> and *Nfat5*<sup>−/−</sup> mice have been described previously (López-Rodríguez et al., 2004), and were cultured in DMEM supplemented with 10% FBS, 10 mM Hepes, and 2 mM L-glutamine. VSV-GFP and MCMV-GFP were kindly provided by Dr. Estanislao Nistal-Villán and Dr. Ana Angulo, respectively. The LCMV strain Docile was from Dr. Andreas Meyerhans.

### Reagents

Poly(I:C) (Cat# tlr-pic) and Pam3CSK4 (Cat# tlr-pms) were from Invivogen; recombinant mouse IFN $\alpha$ 4 was purchased from eBioscience (Cat# 14–8313); recombinant mouse IFN $\alpha$  for in vivo experiments was from Miltenyi Biotec (Cat# 130-093-131); and recombinant mouse IFN $\beta$ 1 was from BioLegend (Cat# 581302). 5-FU (Cat# F6627), formaldehyde, glycine, Trizma base, EDTA,  $\beta$ -glycerophosphate, PMSF, leupeptin, pepstatin A, aprotinin, SDS,  $\beta$ -mercaptoethanol, and TX-100 were from Sigma-Aldrich. Sodium fluoride was from Merck.

### RAW 264.7 transfection and reporter assays

RAW 264.7 mouse macrophage cell line was from ATCC and provided by Dr. Annabel Valledor (Universitat de Barcelona, Barcelona, Spain). Cells were negative for mycoplasma contamination in routine periodic tests in our laboratory. 10  $\times$  10<sup>6</sup> RAW 264.7 macrophage cells were transfected by electroporation in 0.4-cm gap cuvettes (Bio-Rad) at 320 V and 975  $\mu$ F in a Bio-Rad Gene Pulser. For each transfection, a total of 25  $\mu$ g of plasmid DNA was transfected including 8  $\mu$ g of the indicated

luciferase-expressing plasmids in each case and 2  $\mu$ g of pRL-TK (Promega, Cat# E2231) as an internal control for electroporation efficiency. For shRNA transfection, 15  $\mu$ g of shNFAT5 or shGFP (Buxadé et al., 2012) were transfected. For experiments using *IFNBI*-Luc or its mutant forms, 8  $\mu$ g of each reporter plus 2  $\mu$ g of pRL-TK were transfected with 15  $\mu$ g of pBlueScript (Stratagene, currently available from Addgene, Cat# 212207) as a carrier. 10  $\mu$ g of NFAT5-DBD-GFP expression plasmid or its control GFP expression plasmid (López-Rodríguez et al., 2001) were transfected together with 5  $\mu$ g of pBlueScript as a carrier. 18 h after transfection, RAW 264.7 cells were stimulated with poly(I:C) for 6 h and then lysed (Passive Lysis Buffer, Promega, Cat# E1941) to measure luciferase activity using the Renilla Luciferase Assay System (Promega, Cat# E2810) following manufacturer's instructions.

### Reporter plasmids and mutagenesis

The *IFNBI*-Luc reporter (driven by the proximal 123 bps of human *IFNBI* promoter) was provided by Dr. Angel Corbí (Centro de Investigaciones Biológicas, Consejo Superior de Investigaciones Científicas, Madrid, Spain), and the PRDIII-I-Luc and PRDII-Luc reporters were from Dr. Tom Maniatis (Columbia University, New York, NY) and Dr. Benjamin tenOever (Icahn School of Medicine, New York, NY). Mutations in *IFNBI*-Luc reporter (see Fig. 7 D for a description of these mutants) were introduced with the primers listed in Table S3 with the corresponding base pair changes. The protocol was adapted from the QuikChange Site-Directed Mutagenesis kit (Agilent). Briefly, mutant strand synthesis reaction was done using Phusion High-Fidelity DNA Polymerase (New England Biolabs, Cat# M0530S), followed by the purification of PCR product with QIAquick Gel Extraction Kit (Qiagen, Cat# 28704) and digestion with DpnI (Roche, Cat# 10742970001) for 2 h at 37°C. Purified products were then transformed by a 1-min heat pulse in DH5 $\alpha$ -competent cells and plated to grow overnight in ampicillin-containing LB agar plates. Clones were validated by Sanger sequencing (Genomics Facility, Universitat Pompeu Fabra) and prepared for transfection using the Plasmid Maxi Kit (Qiagen, Cat# 12163).

### mRNA quantification by RT-qPCR

Total RNA from cultured cells was extracted with the High Pure RNA Isolation System (Roche, Cat# 11828665001), quantified in a NanoDrop (ND-1000) spectrophotometer and retrotranscribed to cDNA using a Transcriptor First Strand cDNA synthesis system with random primers (Roche, Cat# 04897030001). Total RNA from in vivo sorted cells was extracted using the RNeasy Microkit (Qiagen, Cat# 74004), and the RNA was retrotranscribed using the SuperScript III First-Strand Synthesis system (Thermo Fisher Scientific, Cat# 18080051). For RT-qPCR, LightCycler 480 SYBR Green I Master (Roche, Cat# 4887352001), LightCycler 480 Multiwell Plate (Roche, Cat# 04729749001), and the LightCycler 480 Real-Time PCR System (Roche) were used according to the instructions provided by the manufacturers. All samples were normalized to *L32* mRNA levels using the LightCycler Software, version 1.5. Primers used for RT-qPCR analysis are listed in Table S3.

### Microarray analysis

Total RNA was extracted (RNeasy Microkit; Qiagen, Cat# 74004) from wild-type and NFAT5-deficient BMDMs left untreated or treated with poly(I:C) (6 h, 1 or 0.2 µg/ml). For microarray analysis, amplification, labeling, and hybridizations were performed according to protocol GeneChip WT PLUS Reagent kit (P/N 703174 Rev. 2) and then hybridized to GeneChip Mouse Gene 2.0 ST Array (Affymetrix) in a GeneChip Hybridization Oven 640. Washing and scanning were performed using the Hybridization Wash and Stain Kit and the GeneChip System of Affymetrix (GeneChip Fluidics Station 450 and GeneChip Scanner 3000 7G) according to the Expression Wash, Stain and Scan User Manual (P/N 702731 Rev. 3). After quality control of raw data, the background was corrected, quantile was normalized, and data were summarized to a gene-level using the robust multi-chip average (Irizarry et al., 2003), obtaining a total of 34,390 transcript clusters, excluding controls, which roughly correspond to genes. NetAffx 33.2 annotations, mouse genome 10 built, were used to summarize data into transcript clusters and to annotate analyzed data. Linear Models for Microarray (Smyth, 2004), a moderated *t*-statistics model, was used for detecting differentially expressed genes between the conditions. Correction for multiple comparisons was performed using false discovery rate (Benjamini and Hochberg, 1995). Genes with an adjusted *P* value <0.05 and with an absolute fold-change value >1.5 were selected as significant. All data analysis was performed in R (version 3.0.2) with the following packages: *aroma.affymetrix* to normalize data (Bengtsson et al., 2008), *Biobase* for general data treatment, and *Linear Models for Microarray* to perform differentially expressed analysis. GSEA was used to perform functional analysis (Subramanian et al., 2005; Mootha et al., 2003). This method links the obtained microarray expression profile with GSs available in the Molecular Signatures Database. The classical GSEA analysis was performed with collections Hallmark, C2, C5, and C7, with default parameters and permutation on the gene\_sets. GSs with a *P* value <0.05 and false discovery rate *q* value <0.25 were selected. Analysis of the list of significant differentially expressed genes in the Interferome database v2.01 (Rusinova et al., 2013) was done by filtering the search criteria to IFN- $\gamma$ , genes responsive to IFN $\alpha$ ,  $\beta$ , or both, and *Mus musculus*. The Gene Expression Omnibus accession no. for the microarray set is GSE124287.

### Western blot

10<sup>6</sup> BMDMs were lysed in 100 µl TX-100 lysis buffer (1% TX-100, 40 mM Hepes, pH 7.4, 120 mM NaCl, 1 mM EDTA, 1 mM PMSF, 5 mg/ml aprotinin, 5 mg/ml leupeptin, 1 mg/ml pepstatin A, 1 mM NaF, 1 mM sodium orthovanadate, 10 mM sodium pyrophosphate, and 10 mM  $\beta$ -glycerophosphate). Protein concentration was quantified using the BCA assay (Thermo Fisher Scientific, Cat# 23227), and lysates were boiled in reducing Laemmli buffer. Proteins were subjected to SDS-PAGE and transferred to Protran membranes (Schleicher & Schuell, Cat# BA83). Membranes were blocked with 5% dry milk or 2.5% BSA in Tris-buffered saline (TBS) and immunoblotted with specific primary antibodies in TBS-Tween 0.05%. Antibodies used are indicated below. Membranes were then washed with TBS-

Tween 0.05% and incubated with anti-rabbit Ig or anti-mouse Ig peroxidase-conjugated secondary antibody (GE Healthcare). After washing with TBS-Tween 0.05%, immunoreactive bands were visualized using enhanced chemiluminescence reagents (ECL Western Blotting Detection Reagents; Amersham, Cat# RPN2106). Primary antibodies used were anti-NFAT5 (Affinity BioReagents, Cat# PA1-123), anti-phospho-Y701-STAT1 (BD Biosciences, Cat# 612132), anti-STAT1 (BD Biosciences, Cat# 610119), anti-phospho-S396-IRF3 (Cell Signaling, Cat# 4947S), and anti-pyruvate kinase (Abcam, Cat# Ab191). Western blot quantification was done with ImageJ/Multi Gauge software (Fujifilm).

### ELISA

Cell-free supernatants from BMDM cultures were analyzed for IFN $\beta$  production using the Verikine Mouse IFN Beta ELISA Kit (PBL, Cat# 42400-1), following the manufacturer's instructions. The concentration of IFN $\alpha$  in serum was analyzed using the Mouse IFN  $\alpha$  ELISA Kit (Invitrogen, Cat# BMS6027) according to the instructions provided by the manufacturer.

### ChIP

BMDMs were cultured in 15-cm-diameter polystyrene dishes (18–20 × 10<sup>6</sup> cells) and either left untreated or stimulated with poly(I:C) (1 µg/ml for 2.5 h) before their fixation with 0.75% formaldehyde for 10 min at room temperature. Formaldehyde was then quenched with glycine (final concentration 0.26 M) for 5 min. After washing the plates twice with cold PBS, cells were collected with cell scrapers and lysed in 0.5 ml of lysis buffer (1% SDS, 10 mM EDTA, 50 mM Tris-HCl, pH 8, 1 mM PMSF, 5 µg/ml leupeptin/aprotinin, 1 µg/ml pepstatin A, 10 mM NaF, 10 mM sodium orthovanadate, and 10 mM  $\beta$ -glycerophosphate) for 30 min, rotating at room temperature. Lysates were sonicated using the Diagenode Bioruptor sonication system (UCD-200TM-EX). Each sample was divided into two 1.5-ml tubes containing 250 µl of lysate and sonicated for six cycles (30 s on, 30 s off) at the high power setting to obtain DNA fragments between 500 and 1,000 bp. After sonication, samples were centrifuged to remove insoluble debris, supernatants were collected, and 5% of each sample was used to measure chromatin input. The rest of the sample was diluted 1:10 in ChIP dilution buffer (1% TX-100, 20 mM Tris-HCl, pH 8, 2 mM EDTA, 150 mM NaCl, 1 mM PMSF, 5 µg/ml leupeptin, 5 µg/ml aprotinin, 1 µg/ml pepstatin A, 10 mM NaF, 10 mM sodium orthovanadate, and 10 mM  $\beta$ -glycerophosphate) for immunoprecipitation. Samples were pre-cleared with protein A Sepharose beads (GE Healthcare, Cat# 17-0780-01) that were previously pre-adsorbed with fish sperm DNA (Roche, Cat# 11467140001) and BSA (New England Biolabs, Cat# B9001S) for 1 h at 4°C. Specific antibodies were added to the lysates after removing the preclearing beads and incubated overnight at 4°C. Pre-adsorbed protein A Sepharose beads (GE Healthcare) were then added, incubated for 1 h at 4°C, and then washed three times with ChIP washing buffer (0.1% SDS, 1% TX-100, 20 mM Tris-HCl, pH 8, 2 mM EDTA, and 150 mM NaCl) and once with final washing buffer (0.1% SDS, 1% TX-100, 20 mM Tris-HCl pH 8, 2 mM EDTA, and 500 mM NaCl). To elute the DNA, beads were gently shaken with 200 µl of elution buffer

(1% SDS and 100 mM NaHCO<sub>3</sub>) for 30 min at room temperature. To reverse the cross-linking, samples were incubated overnight at 65°C. Samples were then incubated with 6 ng/μl RNase (Roche) for 30 min at 37°C, incubated for 1 h at 50°C after adding 350 μg/ml of Proteinase K (Roche), and DNA was purified by ethanol precipitation. Antibodies used for ChIP were the following: NFAT5 was detected using a mixture of two rabbit polyclonal antibodies to the amino-terminal region and the DBD region (López-Rodríguez et al., 1999), and preimmune serum served as control; anti-IRF3 (Santa Cruz Biotechnology, Cat# sc-9082); anti-p65 (Santa Cruz Biotechnology, Cat# sc-372); anti-histone H4 (Diagenode, Cat# C15410156-50); anti-acetyl-histone H4 (Millipore, Cat# 06-866), and rabbit IgG (Santa Cruz Biotechnology, Cat# sc-2027). ChIP and its inputs were analyzed by RT-qPCR using the primers listed in Table S3, and the immunoprecipitated DNA from each sample was normalized to its respective chromatin input. RT-qPCR analysis was done with LightCycler Software version 1.5.

### Flow cytometry

All experiments were analyzed at the Flow Cytometry core facility of Universitat Pompeu Fabra using the LSRII (BD Biosciences) equipped with a 488-nm laser, a 633-nm laser and a 407-nm laser, or the LSR FORTRESSA (BD Biosciences) equipped with a 488-nm laser, a 561-nm laser, a 633-nm laser, and a 405-nm laser. For sorting, cell suspensions were filtered through a 35-μm nylon mesh (Falcon, Cat# 352235) and sorted in a BD FACS ARIA cell sorter equipped with 488-nm, 561-nm, 633-nm, and 405-nm lasers. For bone marrow precursors and HSC analysis, femoral and tibial marrow were flushed from the bones to enrich for lineage-negative progenitor populations, and bone marrow cells were first stained with a biotin-conjugated lineage markers cocktail (CD3, CD11b, B220, Ly6G, and TER119) and Mouse Hematopoietic Lineage Biotin Panel (eBioscience, Cat# 88-7774-75), followed by depletion with Streptavidin particles plus - DM (BD Biosciences, Cat# 557812). Exclusion of dead cells was done by staining with the fluorescent dye DAPI (1 μg/ml; BD Biosciences, Cat# 564907) and gating out the positive cells. Apoptotic cells were detected by flow cytometry after incubation with 2 μl/ml of Annexin-V-FLUOS (Roche, Cat# 11828681001) and 1 μg/ml DAPI (BD Biosciences, Cat# 564907) in complete DMEM after staining with surface marker antibodies. Annexin V-positive cells were analyzed in the DAPI-negative population. Flow cytometry antibodies and other reagents (annexin V, DAPI, and streptavidin) are listed in Table S4. For intracellular staining of Ki67 or phospho-STAT1, the Foxp3/Transcription factor fixation/permeabilization buffer (eBioscience, Cat# 00-5521) and permeabilization buffer (eBioscience, Cat# 00-8333-56) were used following the one-step protocol for intracellular proteins from eBioscience. All experiments were analyzed with FACS-Diva version 6.2 software (BD Biosciences). Gating strategies for flow cytometry and cell sorting are shown in Figs. S2, A and B; and S3 A.

### Analysis of NFAT5-IRF DNA binding competition

Binding assays were done using bacterially produced recombinant DBDs of human NFAT5 (aa 175–471), wild-type IRF3 (aa 1–112), a DNA binding mutant of IRF3 with Ala substitutions in

Arg78 and Arg81, and wild-type IRF7 (aa 1–134). NFAT5-DBD was used as a GST-tagged protein (GST-NFAT5-DBD), as we had previously validated it in *in vitro* DNA-binding experiments (Esensten et al., 2005) and having the GST tag was convenient for the binding assay. The respective IRF DBDs were produced as 6His-tagged proteins, then had the 6His tag removed with thrombin or PreScission protease, and were purified again. The respective bacterial expression constructs and purification methods have been described previously (López-Rodríguez et al., 2001; Escalante et al., 2007). Purified recombinant wild-type IRF3 and IRF7 DBDs were kindly provided by Dr. Carlos R. Escalante, and additional wild-type IRF3 and its double mutant Arg78Ala Arg81Ala DBD were produced at the Biomolecular Screening & Protein Technologies Unit of the Centre for Genomic Regulation (Barcelona, Spain). Biotin-tagged (5'-end) double-strand DNA oligonucleotides spanning the PRDIII site, which contains overlapping binding sequences for NFAT5 and IRF in the human *IFNB1* enhancosome, were from Integrated DNA Technologies. A wild-type and a mutant oligonucleotide probe with the NFAT5-binding site disrupted (NFAT5mut) were used in the binding assays and are listed in Table S3.

Assays to assess the competition between NFAT5 and IRF3 or IRF7 for binding to the PRDIII site were done as follows. First, NFAT5-DBD (GST-NFAT5-DBD, 1.4 μg per binding reaction, in a final volume of 20 μl) was incubated with poly(dI):poly(dC) (20 μg/ml) for 60 min at 4°C in binding buffer (5% glycerol, 10 mM Hepes, 100 mM NaCl, 0.8 mg/ml BSA, and 1 mM dithiothreitol, pH 7.3) to prevent nonspecific binding to the oligonucleotide probe. Biotin-tagged double-strand DNA oligonucleotides (oligonucleotide probe) were then added to the reaction (0.8 μg of oligonucleotide probe per reaction) and further incubated for 90 min at 30°C, plus 30 min at 25°C. Reactions were tested with different molar ratios of NFAT5-DBD to oligonucleotide probe (from 1:30 to 1:1), and a ratio of 1:6 for GST-NFAT5-DBD to oligonucleotide probe was selected as it yielded an optimal binding signal. Then, GST-NFAT5-DBD was captured with glutathione-Sepharose 4B beads (GE Healthcare, Cat# 17-0756-01) added to the reaction and incubated for 60 min at 4°C. The equivalent of 0.2 μl of bead slurry was used per sample, and beads were previously filtered (Falcon 70-μm filters, BD Biosciences, Cat# 340606) to remove large particles that could obstruct the cytometer. Beads with captured NFAT5-DNA complexes were then washed with binding buffer to remove unbound biotin-ds-oligo, resuspended in 100 μl of binding buffer and incubated with 3 μg of streptavidin conjugated with eFluor 450 (eBioscience, Cat# 48-4317-82) for 30 min at 4°C. Beads were then washed twice with PBS, resuspended in 300 μl of PBS, and transferred to flow cytometer tubes for analysis. For competition assays between NFAT5-DBD and IRF-DBDs, the biotin-ds-oligo was preincubated with the respective IRFs for 45 min at 30°C before adding NFAT5-DBD to the binding reaction. IRF-DBDs were used in a 4:1 molar excess with respect to NFAT5-DBD.

### Sequence alignment

Jalview (Waterhouse et al., 2009) was used for alignment of the *IFNB1* promoter region in the genomes of different mammalian species.



## Statistical analysis

All data are presented as mean  $\pm$  SEM. Data were analyzed with GraphPad Prism 6 software. Normality (Gaussian distribution) of samples was determined by a D'Agostino-Pearson normality test before calculating statistical significance with an unpaired *t* test (for sets of samples with a Gaussian distribution) or Mann-Whitney test (samples with a non-Gaussian distribution). A one-sample *t* test was used when samples were compared with a reference control sample (set to an arbitrary value of 1 or 100). Specific statistics analyses, number of samples, and independent experiments done are indicated in each respective figure legend.

## Online supplemental material

Fig. S1 (related to Fig. 1) includes the following bioinformatics analysis of the microarray data: GSEA analysis of the IFN $\gamma$  and apoptosis responses, and a volcano plot with all the ISG genes differentially expressed between poly(I:C)-treated NFAT5-deficient and control macrophages. It also illustrates the expression of NFAT5 upon poly(I:C) and IFN $\alpha$  treatments, and analysis of STAT1 expression and phosphorylation (Y701) in wild-type and NFAT5-deficient BMDMs. Fig. S2 (related to Figs. 2 and 3) illustrates the gating strategies used to isolate pDCs and macrophages from spleens and bone marrow of LCMV-infected mice, and includes a panel showing that infected NFAT5-deficient and control mice have similar numbers of diverse innate immunity cells. This figure also describes the expression of a group of ISGs in pDCs and macrophages from NFAT5-deficient and control mice 3 d after in vivo LCMV infection. Fig. S2 includes the expression of IFN-I-related genes in in vitro-infected NFAT5-deficient and control conventional DCs and also shows cell-intrinsic and paracrine effects of the NFAT5-mediated IFN-I repression upon infection. Fig. S3 (related to Fig. 4) illustrates the flow cytometry gating strategy used to analyze percentages of the HSPC and HSC cycle profile and shows the percentages of NFAT5-deficient LSK and MPP3/4 and proportion of quiescent Ki67-negative HSCs in NFAT5-deficient mice in response to poly(I:C) and IFN $\alpha$ . This figure also shows the expression of ISG in HSCs from myeloid-specific NFAT5-deficient mice. Fig. S4 (related to Fig. 4) shows hematologic and bone marrow progenitor cell parameters in wild-type and NFAT5-deficient mice upon acute LCMV infection. Table S1 shows the list of Interferome database genes differentially expressed between poly(I:C)-treated wild-type and NFAT5-deficient macrophages. Table S2 shows comparable expression of genes encoding for components of TLR and IFN-I signaling in wild-type and NFAT5-deficient macrophages. Table S3 is a list of primers and oligonucleotide probes used in this work. Table S4 lists antibodies and reagents used for flow cytometry and cell isolation.

## Acknowledgments

We thank Tom Maniatis (Columbia University Medical Center, New York, NY) and Benjamin tenOever (Icahn School of Medicine, New York, NY) for 3 $\times$  PRDIII-I and 2 $\times$  PRDII reporters, Angel Corbí (Centro de Investigaciones Biológicas, Consejo Superior de Investigaciones Científicas, Madrid, Spain) for the IFN $\beta$  reporter, and Annabel Valledor (University of Barcelona,

Barcelona, Spain) for the RAW 264.7 macrophage cell line. We are grateful to Manuel Rebelo (Gulbenkian Institute, Oeiras, Portugal) for providing the *Ifnar*<sup>-/-</sup> mice. Gabriel Gil (Institut Hospital del Mar d'Investigacions Mèdiques [IMIM], Barcelona, Spain) is acknowledged for the anti-CD11b hybridoma M1/70.15. We thank Mireia Pedragosa (Universitat Pompeu Fabra [UPF], Barcelona, Spain) for advice with in vivo LCMV infections; Berta Canal de Torres (UPF) for guidance with the mutagenesis approaches; Marcel Costa (UPF), Lara Nonell, Eulalia Puigdecamet (Servei d'Anàlisi de Microarrays, IMIM), and Juan José Lozano (Centro de Investigación Biomédica en Red de Enfermedades Hepáticas y Digestivas, Barcelona, Spain) for microarray hybridization and bioinformatics analysis; Manuel Irimia (Center for Genomic Regulation, Barcelona, Spain) and Nacho Maeso (Centro Andaluz de Biología del Desarrollo, Sevilla, Spain) for advice with sequence alignment; Oscar Fornas and Roger Anglada for advice with experiments using the UPF Flow Cytometry and Genomics facilities; and Carlo Carolis and Natalia Rodrigo (Screening & Protein Technologies Unit of the Center for Genomic Regulation, Barcelona, Spain) for production of different IRF3 proteins. We thank Anna Bigas and José Yélamos (IMIM) for advice with HSC analysis. We also thank María García Belando and Alba Deyá for excellent technical support with maintenance and genotyping of mouse colonies.

This work was supported by the Agencia Estatal de Investigación, Spanish Ministry of Economy and Competitiveness, and FEDER (SAF2015-71363-R and RTI2018-095902-B-I00 to C. López-Rodríguez and J. Aramburu; and SAF2016-75505-R to A. Meyerhans and J. Argilaguet), and Fundació la Marató TV3 (1225-30 and 201619-30) to C. López-Rodríguez and J. Aramburu. We also acknowledge funding support from Generalitat de Catalunya (2014SGR1153 and 2017SGR888) and the Spanish Ministry of Economy and Competitiveness through the "María de Maeztu" Program for Units of Excellence in R&D (MDM-2014-0370). H. Huerga Encabo was supported by a predoctoral fellowship of the Spanish Ministry of Education, Culture and Sports (FPU13/01798), and L. Traveset was supported by a predoctoral fellowship of the Spanish Ministerio de Economía, Industria and Competitiveness (BES-2015-074170). C. López-Rodríguez is a recipient of an ICREA Acadèmia award from Institució Catalana de Recerca i Estudis Avançats (Generalitat de Catalunya).

The authors declare no competing financial interests.

Author contributions: H. Huerga Encabo designed, performed, and analyzed the majority of the experimental work, prepared the figures, and contributed to manuscript writing; L. Traveset did most of the Western blots, participated in the hematological and HSC analyses, and in setting up the NFAT5-IRF competition assays; J. Argilaguet and A. Meyerhans provided expertise with the in vivo infections and analyzed the viral load; E. Nistal-Villán provided the VSV and guidance with this model; R. Jaiswal and C.R. Escalante contributed with the production of recombinant IRF proteins. A. Angulo provided the MCMV and guidance with this model; C. Gekas provided guidance with the analysis of HSCs; J. Aramburu contributed with experimental design and analysis, manuscript writing, and figure preparation; C. López-Rodríguez designed and supervised the work, analyzed

the results and interpreted the data, prepared the figures, and wrote the manuscript.

Submitted: 12 March 2019

Revised: 23 September 2019

Accepted: 7 November 2019

## References

- Agaloti, T., S. Lomvardas, B. Parekh, J. Yie, T. Maniatis, and D. Thanos. 2000. Ordered recruitment of chromatin modifying and general transcription factors to the IFN-beta promoter. *Cell*. 103:667–678. [https://doi.org/10.1016/S0092-8674\(00\)00169-0](https://doi.org/10.1016/S0092-8674(00)00169-0)
- Akira, S., S. Uematsu, and O. Takeuchi. 2006. Pathogen recognition and innate immunity. *Cell*. 124:783–801. <https://doi.org/10.1016/j.cell.2006.02.015>
- Alberdi, M., M. Iglesias, S. Tejedor, R. Merino, C. López-Rodríguez, and J. Aramburu. 2017. Context-dependent regulation of Th17-associated genes and IFN $\gamma$  expression by the transcription factor NFAT5. *Immunol. Cell Biol.* 95:56–67. <https://doi.org/10.1038/icb.2016.69>
- Aramburu, J., and C. López-Rodríguez. 2019. Regulation of inflammatory functions of macrophages and T lymphocytes by NFAT5. *Front. Immunol.* 10:535. <https://doi.org/10.3389/fimmu.2019.00535>
- Arimoto, K.-I., S. Miyauchi, S.A. Stoner, J.-B. Fan, and D.-E. Zhang. 2018. Negative regulation of type I IFN signaling. *J. Leukoc. Biol.* 103:1099–1116. <https://doi.org/10.1002/JLB.2MIRO817-342R>
- Bao, M., Y. Wang, Y. Liu, P. Shi, H. Lu, W. Sha, L. Weng, S. Hanabuchi, J. Qin, J. Plumas, et al. 2016. NFATC3 promotes IRF7 transcriptional activity in plasmacytoid dendritic cells. *J. Exp. Med.* 213:2383–2398. <https://doi.org/10.1084/jem.20160438>
- Barchet, W., M. Cella, B. Odermatt, C. Asselin-Paturel, M. Colonna, and U. Kalinke. 2002. Virus-induced interferon alpha production by a dendritic cell subset in the absence of feedback signaling in vivo. *J. Exp. Med.* 195:507–516. <https://doi.org/10.1084/jem.20011666>
- Battegay, M., S. Cooper, A. Althage, J. Bänziger, H. Hengartner, and R.M. Zinkernagel. 1991. Quantification of lymphocytic choriomeningitis virus with an immunological focus assay in 24- or 96-well plates. *J. Virol. Methods*. 33:191–198. [https://doi.org/10.1016/0166-0934\(91\)90018-U](https://doi.org/10.1016/0166-0934(91)90018-U)
- Bengtsson, H., K. Simpson, J. Bullard, and K. Hansen. 2008. aroma.affymetrix: A generic framework in R for analyzing small to very large Affymetrix data sets in bounded memory. Technical Report, 745. Department of Statistics, University of California, Berkeley. Available at: <https://statistics.berkeley.edu/sites/default/files/tech-reports/745.pdf>
- Benjamini, Y., and Y. Hochberg. 1995. Controlling the false discovery rate: a practical and powerful approach to multiple testing. *Journal of the Royal Statistical Society*. 57:289–300.
- Bernitz, J.M., H.S. Kim, B. MacArthur, H. Sieburg, and K. Moore. 2016. Hematopoietic stem cells count and remember self-renewal divisions. *Cell*. 167:1296–1309.e10. <https://doi.org/10.1016/j.cell.2016.10.022>
- Borrow, P., L. Martínez-Sobrido, and J.C. de la Torre. 2010. Inhibition of the type I interferon antiviral response during arenavirus infection. *Viruses*. 2:2443–2480. <https://doi.org/10.3390/v2112443>
- Buxadé, M., G. Lunazzi, J. Minguillón, S. Iborra, R. Berga-Bolaños, M. Del Val, J. Aramburu, and C. López-Rodríguez. 2012. Gene expression induced by Toll-like receptors in macrophages requires the transcription factor NFAT5. *J. Exp. Med.* 209:379–393. <https://doi.org/10.1084/jem.20111569>
- Buxadé, M., H. Huerga Encabo, M. Riera-Borrull, L. Quintana-Gallardo, P. López-Cotarelo, M. Tellechea, S. Martínez-Martínez, J.M. Redondo, J. Martín-Caballero, J.M. Flores, et al. 2018. Macrophage-specific MHCII expression is regulated by a remote Ciita enhancer controlled by NFAT5. *J. Exp. Med.* 215:2901–2918. <https://doi.org/10.1084/jem.20180314>
- Chen, J., E. Baig, and E.N. Fish. 2004. Diversity and relatedness among the type I interferons. *J. Interferon Cytokine Res.* 24:687–698. <https://doi.org/10.1089/jir.2004.24.687>
- Cousens, L.P., R. Peterson, S. Hsu, A. Dorner, J.D. Altman, R. Ahmed, and C.A. Biron. 1999. Two roads diverged: interferon alpha/beta- and interleukin 12-mediated pathways in promoting T cell interferon gamma responses during viral infection. *J. Exp. Med.* 189:1315–1328. <https://doi.org/10.1084/jem.189.8.1315>
- Escalante, C.R., L. Shen, D. Thanos, and A.K. Aggarwal. 2002. Structure of NF-kappaB p50/p65 heterodimer bound to the PRDII DNA element from the interferon-beta promoter. *Structure*. 10:383–391. [https://doi.org/10.1016/S0969-2126\(02\)00723-2](https://doi.org/10.1016/S0969-2126(02)00723-2)
- Escalante, C.R., E. Nistal-Villán, L. Shen, A. García-Sastre, and A.K. Aggarwal. 2007. Structure of IRF-3 bound to the PRDIII-I regulatory element of the human interferon- $\beta$  enhancer. *Mol. Cell*. 26:703–716. <https://doi.org/10.1016/j.molcel.2007.04.022>
- Esensten, J.H., A.V. Tsytsykova, C. Lopez-Rodriguez, F.A. Ligeiro, A. Rao, and A.E. Goldfeld. 2005. NFAT5 binds to the TNF promoter distinctly from NFATp, c, 3 and 4, and activates TNF transcription during hypertonic stress alone. *Nucleic Acids Res.* 33:3845–3854. <https://doi.org/10.1093/nar/gki701>
- Essers, M.A.G., S. Offner, W.E. Blanco-Boise, Z. Waibler, U. Kalinke, M.A. Duchosal, and A. Trumpp. 2009. IFNalpha activates dormant haematopoietic stem cells in vivo. *Nature*. 458:904–908. <https://doi.org/10.1038/nature07815>
- Gilchrist, M., V. Thorsson, B. Li, A.G. Rust, M. Korb, J.C. Roach, K. Kennedy, T. Hai, H. Bolouri, and A. Aderem. 2006. Systems biology approaches identify ATF3 as a negative regulator of Toll-like receptor 4. *Nature*. 441:173–178. <https://doi.org/10.1038/nature04768>
- Guarda, G., M. Braun, F. Staehli, A. Tardivel, C. Mattmann, I. Förster, M. Farlik, T. Decker, R.A. Du Pasquier, P. Romero, and J. Tschoopp. 2011. Type I interferon inhibits interleukin-1 production and inflammasome activation. *Immunity*. 34:213–223. <https://doi.org/10.1016/j.immuni.2011.02.006>
- Honda, K., and T. Taniguchi. 2006. IRFs: master regulators of signalling by Toll-like receptors and cytosolic pattern-recognition receptors. *Nat. Rev. Immunol.* 6:644–658. <https://doi.org/10.1038/nri1900>
- Honda, K., H. Yanai, H. Negishi, M. Asagiri, M. Sato, T. Mizutani, N. Shimada, Y. Ohba, A. Takaoka, N. Yoshida, and T. Taniguchi. 2005. IRF-7 is the master regulator of type-I interferon-dependent immune responses. *Nature*. 434:772–777. <https://doi.org/10.1038/nature03464>
- Honda, K., A. Takaoka, and T. Taniguchi. 2006. Type I interferon [corrected] gene induction by the interferon regulatory factor family of transcription factors. *Immunity*. 25:349–360. <https://doi.org/10.1016/j.immuni.2006.08.009>
- Irizarry, R.A., B. Hobbs, F. Collin, Y.D. Beazer-Barclay, K.J. Antonellis, U. Scherf, and T.P. Speed. 2003. Exploration, normalization, and summarization of high density oligonucleotide array probe level data. *Biostatistics*. 4:249–264. <https://doi.org/10.1093/biostatistics/4.2.249>
- Ivashkiv, L.B., and L.T. Donlin. 2014. Regulation of type I interferon responses. *Nat. Rev. Immunol.* 14:36–49. <https://doi.org/10.1038/nri3581>
- Jantsch, J., V. Schatz, D. Friedrich, A. Schröder, C. Kopp, I. Siegert, A. Maronna, D. Wendelborn, P. Linz, K.J.J. Binger, et al. 2015. Cutaneous Na+ storage strengthens the antimicrobial barrier function of the skin and boosts macrophage-driven host defense. *Cell Metab.* 21:493–501. <https://doi.org/10.1016/j.cmet.2015.02.003>
- King, K.Y., and M.A. Goodell. 2011. Inflammatory modulation of HSCs: viewing the HSC as a foundation for the immune response. *Nat. Rev. Immunol.* 11:685–692. <https://doi.org/10.1038/nri3062>
- Labzin, L.I., S.V. Schmidt, S.L. Masters, M. Beyer, W. Krebs, K. Klee, R. Stahl, D. Lütjohann, J.L. Schultze, E. Latz, and D. De Nardo. 2015. ATF3 is a key regulator of macrophage IFN responses. *J. Immunol.* 195:4446–4455. <https://doi.org/10.4049/jimmunol.1500204>
- Lerner, C., and D.E. Harrison. 1990. 5-Fluorouracil spares hemopoietic stem cells responsible for long-term repopulation. *Exp. Hematol.* 18:114–118.
- Levy, D.E., I.J. Marié, and J.E. Durbin. 2011. Induction and function of type I and III interferon in response to viral infection. *Curr. Opin. Virol.* 1:476–486. <https://doi.org/10.1016/j.coviro.2011.11.001>
- Lopez-Rodríguez, C., J. Aramburu, A.S. Rakeman, and A. Rao. 1999. NFAT5, a constitutively nuclear NFAT protein that does not cooperate with Fos and Jun. *Proc. Natl. Acad. Sci. USA*. 96:7214–7219. <https://doi.org/10.1073/pnas.96.13.7214>
- López-Rodríguez, C., J. Aramburu, L. Jin, A.S. Rakeman, M. Michino, and A. Rao. 2001. Bridging the NFAT and NF-kappaB families: NFAT5 dimerization regulates cytokine gene transcription in response to osmotic stress. *Immunity*. 15:47–58. [https://doi.org/10.1016/S1074-7613\(01\)00165-0](https://doi.org/10.1016/S1074-7613(01)00165-0)
- López-Rodríguez, C., C.L. Antos, J.M. Shelton, J.A. Richardson, F. Lin, T.I. Novobrantseva, R.T. Bronson, P. Igarashi, A. Rao, and E.N. Olson. 2004. Loss of NFAT5 results in renal atrophy and lack of toxicity-responsive gene expression. *Proc. Natl. Acad. Sci. USA*. 101:2392–2397. <https://doi.org/10.1073/pnas.0308703100>
- MacMicking, J.D. 2012. Interferon-inducible effector mechanisms in cell-autonomous immunity. *Nat. Rev. Immunol.* 12:367–382. <https://doi.org/10.1038/nri3210>

- Marié, I., J.E. Durbin, and D.E. Levy. 1998. Differential viral induction of distinct interferon- $\alpha$  genes by positive feedback through interferon regulatory factor-7. *EMBO J.* 17:6660–6669. <https://doi.org/10.1093/emboj/17.22.6660>
- Matsuyama, T., T. Kimura, M. Kitagawa, K. Pfeffer, T. Kawakami, N. Watanabe, T.M. Kündig, R. Amakawa, K. Kishihara, A. Wakeham, et al. 1993. Targeted disruption of IRF-1 or IRF-2 results in abnormal type I IFN gene induction and aberrant lymphocyte development. *Cell.* 75:83–97. [https://doi.org/10.1016/S0092-8674\(05\)80086-8](https://doi.org/10.1016/S0092-8674(05)80086-8)
- McNab, F., K. Mayer-Barber, A. Sher, A. Wack, and A. O'Garra. 2015. Type I interferons in infectious disease. *Nat. Rev. Immunol.* 15:87–103. <https://doi.org/10.1038/nri3787>
- Merigan, T.C., M.B. Oldstone, and R.M. Welsh. 1977. Interferon production during lymphocytic choriomeningitis virus infection of nude and normal mice. *Nature.* 268:67–68. <https://doi.org/10.1038/268067a0>
- Mootha, V.K., C.M. Lindgren, K.-F. Eriksson, A. Subramanian, S. Sihag, J. Lehar, P. Puigserver, E. Carlsson, M. Ridderstråle, E. Laurila, et al. 2003. PGC-1 $\alpha$ -responsive genes involved in oxidative phosphorylation are coordinately downregulated in human diabetes. *Nat. Genet.* 34:267–273. <https://doi.org/10.1038/ng1180>
- Moskophidis, D., F. Lechner, H. Pircher, and R.M. Zinkernagel. 1993. Virus persistence in acutely infected immunocompetent mice by exhaustion of antiviral cytotoxic effector T cells. *Nature.* 362:758–761. <https://doi.org/10.1038/362758a0>
- Ng, C.T., L.M. Snell, D.G. Brooks, and M.B.A. Oldstone. 2013. Networking at the level of host immunity: immune cell interactions during persistent viral infections. *Cell Host Microbe.* 13:652–664. <https://doi.org/10.1016/j.chom.2013.05.014>
- Nhu, Q.M., N. Cuesta, and S.N. Vogel. 2006. Transcriptional regulation of lipopolysaccharide (LPS)-induced Toll-like receptor (TLR) expression in murine macrophages: role of interferon regulatory factors 1 (IRF-1) and 2 (IRF-2). *J. Endotoxin Res.* 12:285–295. <https://doi.org/10.1177/09680519060120050401>
- O'Neill, L.A.J., and A.G. Bowie. 2007. The family of five: TIR-domain-containing adaptors in Toll-like receptor signalling. *Nat. Rev. Immunol.* 7: 353–364. <https://doi.org/10.1038/nri2079>
- Ooi, A.G.L., H. Karsunky, R. Majeti, S. Butz, D. Vestweber, T. Ishida, T. Quertermous, I.L. Weissman, and E.C. Forsberg. 2009. The adhesion molecule *esam1* is a novel hematopoietic stem cell marker. *Stem Cells.* 27:653–661. <https://doi.org/10.1634/stemcells.2008-0824>
- Oshiumi, H., M. Matsumoto, K. Funami, T. Akazawa, and T. Seya. 2003. TICAM-1, an adaptor molecule that participates in Toll-like receptor 3-mediated interferon- $\beta$  induction. *Nat. Immunol.* 4:161–167. <https://doi.org/10.1038/ni886>
- Panne, D., T. Maniatis, and S.C. Harrison. 2007. An atomic model of the interferon- $\beta$  enhanceosome. *Cell.* 129:1111–1123. <https://doi.org/10.1016/j.cell.2007.05.019>
- Pestka, S., C.D. Krause, and M.R. Walter. 2004. Interferons, interferon-like cytokines, and their receptors. *Immunol. Rev.* 202:8–32. <https://doi.org/10.1111/j.0105-2896.2004.00204.x>
- Pietras, E.M., R. Lakshminarasimhan, J.-M. Techner, S. Fong, J. Flach, M. Binnewies, and E. Passegué. 2014. Re-entry into quiescence protects hematopoietic stem cells from the killing effect of chronic exposure to type I interferons. *J. Exp. Med.* 211:245–262. <https://doi.org/10.1084/jem.20131043>
- Rodero, M.P., and Y.J. Crow. 2016. Type I interferon-mediated monogenic autoinflammation: The type I interferonopathies, a conceptual overview. *J. Exp. Med.* 213:2527–2538. <https://doi.org/10.1084/jem.20161596>
- Rusinova, I., S. Forster, S. Yu, A. Kannan, M. Masse, H. Cumming, R. Chapman, and P.J. Hertzog. 2013. Interferome v2.0: an updated database of annotated interferon-regulated genes. *Nucleic Acids Res.* 41(D1): D1040–D1046. <https://doi.org/10.1093/nar/gks1215>
- Sato, M., N. Tanaka, N. Hata, E. Oda, and T. Taniguchi. 1998. Involvement of the IRF family transcription factor IRF-3 in virus-induced activation of the IFN- $\beta$  gene. *FEBS Lett.* 425:112–116. [https://doi.org/10.1016/S0014-5793\(98\)00210-5](https://doi.org/10.1016/S0014-5793(98)00210-5)
- Sato, T., N. Onai, H. Yoshihara, F. Arai, T. Suda, and T. Ohteki. 2009. Interferon regulatory factor-2 protects quiescent hematopoietic stem cells from type I interferon-dependent exhaustion. *Nat. Med.* 15:696–700. <https://doi.org/10.1038/nm.1973>
- Schneider, W.M., M.D. Chevillotte, and C.M. Rice. 2014. Interferon-stimulated genes: a complex web of host defenses. *Annu. Rev. Immunol.* 32:513–545. <https://doi.org/10.1146/annurev-immunol-032713-120231>
- Senger, K., M. Merika, T. Agalio, J. Yie, C.R. Escalante, G. Chen, A.K. Aggarwal, and D. Thanos. 2000. Gene repression by coactivator repulsion. *Mol. Cell.* 6:931–937. [https://doi.org/10.1016/S1097-2765\(05\)00081-X](https://doi.org/10.1016/S1097-2765(05)00081-X)
- Shahangian, A., E.K. Chow, X. Tian, J.R. Kang, A. Ghaffari, S.Y. Liu, J.A. Belperio, G. Cheng, and J.C. Deng. 2009. Type I IFNs mediate development of postinfluenza bacterial pneumonia in mice. *J. Clin. Invest.* 119: 1910–1920. <https://doi.org/10.1172/JCI35412>
- Smyth, G.K. 2004. Linear models and empirical bayes methods for assessing differential expression in microarray experiments. *Stat. Appl. Genet. Mol. Biol.* 3:e3. <https://doi.org/10.2202/1544-6115.1027>
- Snell, L.M., and D.G. Brooks. 2015. New insights into type I interferon and the immunopathogenesis of persistent viral infections. *Curr. Opin. Immunol.* 34:91–98. <https://doi.org/10.1016/j.coi.2015.03.002>
- Stroud, J.C., C. Lopez-Rodriguez, A. Rao, and L. Chen. 2002. Structure of a TonEBP-DNA complex reveals DNA encircled by a transcription factor. *Nat. Struct. Biol.* 9:90–94. <https://doi.org/10.1038/nsb749>
- Subramanian, A., P. Tamayo, V.K. Mootha, S. Mukherjee, B.L. Ebert, M.A. Gillette, A. Paulovich, S.L. Pomeroy, T.R. Golub, E.S. Lander, and J.P. Mesirov. 2005. Gene set enrichment analysis: a knowledge-based approach for interpreting genome-wide expression profiles. *Proc. Natl. Acad. Sci. USA.* 102:15545–15550. <https://doi.org/10.1073/pnas.0506580102>
- Teijaro, J.R., C. Ng, A.M. Lee, B.M. Sullivan, K.C.F. Sheehan, M. Welch, R.D. Schreiber, J.C. de la Torre, and M.B.A. Oldstone. 2013. Persistent LCMV infection is controlled by blockade of type I interferon signaling. *Science.* 340:207–211. <https://doi.org/10.1126/science.1235214>
- Tellechea, M., M. Buxadé, S. Tejedor, J. Aramburu, and C. López-Rodríguez. 2018. NFAT5-regulated macrophage polarization supports the proinflammatory function of macrophages and T lymphocytes. *J. Immunol.* 200:305–315. <https://doi.org/10.4049/jimmunol.1601942>
- Theofilopoulos, A.N., R. Baccala, B. Beutler, and D.H. Kono. 2005. Type I interferons ( $\alpha/\beta$ ) in immunity and autoimmunity. *Annu. Rev. Immunol.* 23:307–336. <https://doi.org/10.1146/annurev.immunol.23.021704.115843>
- van Pesch, V., H. Lanaya, J.-C. Renauld, and T. Michiels. 2004. Characterization of the murine alpha interferon gene family. *J. Virol.* 78: 8219–8228. <https://doi.org/10.1128/JVI.78.15.8219-8228.2004>
- Waterhouse, A.M., J.B. Procter, D.M.A. Martin, M. Clamp, and G.J. Barton. 2009. Jalview Version 2--a multiple sequence alignment editor and analysis workbench. *Bioinformatics.* 25:1189–1191. <https://doi.org/10.1093/bioinformatics/btp033>
- Wu, J., and Z.J. Chen. 2014. Innate immune sensing and signaling of cytosolic nucleic acids. *Annu. Rev. Immunol.* 32:461–488. <https://doi.org/10.1146/annurev-immunol-032713-120156>
- Yamamoto, M., S. Sato, H. Hemmi, K. Hoshino, T. Kaisho, H. Sanjo, O. Takeuchi, M. Sugiyama, M. Okabe, K. Takeda, and S. Akira. 2003. Role of adaptor TRIF in the MyD88-independent toll-like receptor signaling pathway. *Science.* 301:640–643. <https://doi.org/10.1126/science.1087262>
- Yoneyama, M., W. Suhara, Y. Fukuhara, M. Fukuda, E. Nishida, and T. Fujita. 1998. Direct triggering of the type I interferon system by virus infection: activation of a transcription factor complex containing IRF-3 and CBP/p300. *EMBO J.* 17:1087–1095. <https://doi.org/10.1093/emboj/17.4.1087>
- Zitvogel, L., L. Galluzzi, O. Kepp, M.J. Smyth, and G. Kroemer. 2015. Type I interferons in anticancer immunity. *Nat. Rev. Immunol.* 15:405–414. <https://doi.org/10.1038/nri3845>